

Evolution of the X-ray Emission of Radio-Quiet Quasars

Brandon C. Kelly, Jill Bechtold

Steward Observatory, University of Arizona, 933 N Cherry Ave., Tucson, AZ 85710

`bkelly@as.arizona.edu, jbechtold@as.arizona.edu`

Aneta Siemiginowska, Tom Aldcroft

Harvard-Smithsonian Center for Astrophysics, 60 Garden Street, Cambridge, MA 02138

`asiemiginowska@cfa.harvard.edu, taldcroft@cfa.harvard.edu`

and

Małgorzata Sobolewska

Department of Physics, University of Durham, South Road, DH1 3LE, Durham, UK

`m.a.sobolewska@durham.ac.uk`

ABSTRACT

We report new *Chandra* observations of seven optically faint, $z \sim 4$ radio-quiet quasars. We have combined these new observations with previous *Chandra* observations of radio-quiet quasars to create a sample of 174 sources. These sources have $0.1 < z < 4.7$, and $10^{44} \text{ ergs s}^{-1} < \nu L_\nu(2500\text{\AA}) < 10^{48} \text{ ergs s}^{-1}$. The X-ray detection fraction is 90%. We find that the X-ray loudness of radio-quiet quasars decreases with UV luminosity and increases with redshift. The model that is best supported by the data has a linear dependence of optical-to-X-ray ratio, α_{ox} , on cosmic time, and a quadratic dependence of α_{ox} on $\log L_{UV}$, where α_{ox} becomes X-ray quiet more rapidly at higher $\log L_{UV}$. We find no significant evidence for a relationship between the X-ray photon index, Γ_X , and the UV luminosity, and we find marginally significant evidence that the X-ray continuum flattens with increasing z (2σ). The Γ_X - z anti-correlation may be the result of X-ray spectral curvature, redshifting of a Compton reflection component into the observed *Chandra* band, and/or redshifting of a soft excess out of the observed *Chandra* band. Using the results for Γ_X , we show that the $\alpha_{\text{ox}}-z$ relationship is unlikely to be a spurious result caused by redshifting of the observable X-ray spectral region. A correlation between α_{ox} and z implies evolution of the accretion process. We present a qualitative comparison of these new results with models for accretion disk emission.

Subject headings: accretion disks — quasars: general — ultraviolet: galaxies — X-rays: galaxies — methods:statistical

1. INTRODUCTION

It is widely accepted that the extraordinary activity associated with quasars involves accretion onto a supermassive black hole, with the UV/optical emission arising from a geometrically thin, optically thick cold accretion disk, and the X-ray continuum arising from a hot, optically thin corona that Compton upscatters

the disk’s UV photons. The geometry of the X-ray emitting region is uncertain, but possibilities include an accretion disk that evaporates into a hot inner flow (e.g., Shapiro et al. 1976; Zdziarski et al. 1999), a hot ionized ‘skin’ that sandwiches the cold disk (e.g., Bisnovatyi-Kogan & Blinnikov 1977; Liang & Price 1977; Nayakshin 2000), a combination of a hot inner flow and a corona that sandwiches the disk (e.g., Poutanen et al. 1997; Sobolewska et al. 2004a), or a patchy corona, consisting of a number of hot spots above the accretion disk (e.g., Galeev et al. 1979; Malzac et al. 2001; Sobolewska et al. 2004b). In addition, the UV and X-ray producing processes may be coupled as a result of radiation pressure from the UV photons driving a flow from the disk into the corona (Proga 2005). Investigating the relationships between the UV and X-ray emission is an important step towards understanding the origin of the X-ray emission. Furthermore, learning how the X-ray and UV emission change with z provides insight into evolution of the accretion process, quasar black hole mass, and accretion rate.

Many studies have investigated whether α_{ox} , the ratio of X-ray to UV/optical flux, depends on redshift or UV luminosity, L_{UV} (e.g., Avni & Tananbaum 1982; Wilkes et al. 1994; Yuan et al. 1998a; Bechtold et al. 2003; Vignali et al. 2003b; Strateva et al. 2005; Steffen et al. 2006). The parameter α_{ox} is a simple measure of the amount of X-ray radiation, dominated by non-thermal processes, in respect to the amount of UV radiation, dominated by thermal processes. Most studies have concluded that there is no evidence for a redshift dependence of α_{ox} (e.g., Avni & Tananbaum 1986; Wilkes et al. 1994; Strateva et al. 2005), although Bechtold et al. (2003) argued that α_{ox} is significantly correlated with both z and UV luminosity, and Yuan et al. (1998a) found evidence for a slight dependence of α_{ox} on redshift at $z < 0.5$. Vignali et al. (2003b), Strateva et al. (2005, S05), and Steffen et al. (2006, S06) used a partial correlation and regression analysis to conclude that there is no evidence for a dependence of α_{ox} on z , after accounting for the α_{ox} – L_{UV} and L_{UV} – z correlations. These authors also found evidence that RQQs become more X-ray quiet with increasing UV luminosity.

Previous investigations of the X-ray photon index, Γ_X , have also produced mixed results. Bechtold et al. (2003) used a sample of *ROSAT* observations over from Yuan et al. (1998a) and *Chandra* observations of high redshift quasars to conclude that Γ_X is correlated with both luminosity and z . A Γ_X – L_{UV} correlation was also seen by Dai et al. (2004), using a sample of gravitationally-lensed sources with *XMM-Newton* and *Chandra* data. Some evidence for an anti-correlation between Γ_X and z has also been found using *ASCA* observations (Reeves et al. 1997; Vignali et al. 1999) and *XMM-Newton* observations (Page et al. 2003). However, other investigations based on *XMM-Newton* data (e.g., Risaliti & Elvis 2005) and spectral fitting of composite spectra from *Chandra* observations (e.g., Vignali et al. 2003c, 2005; Shemmer et al. 2006) have not revealed any evidence for a relationship between Γ_X , L_{UV} , and z . Similarly, other *ASCA* observations have also not produced evidence for a Γ_X – z correlation (Reeves & Turner 2000). In addition, there has been evidence for a correlation between Γ_X and the Eddington ratio (e.g., Lu & Yu 1999; Wang et al. 2004; Shemmer et al. 2006), and Gallagher et al. (2005) found evidence for an anti-correlation between Γ_X and the UV spectral slope.

All of these conclusions are by necessity based on flux-limited samples. Flux-limited samples typically suffer from an artificial correlation between z and L_{UV} , making it difficult to disentangle which parameter is more important in determining X-ray properties. To help break the L_{UV} – z degeneracy, we observed seven optically faint $z \sim 4$ radio-quiet quasars with *Chandra*. We combined these sources with *Chandra* data of optically-selected radio-quiet quasars, drawn mostly from the Sloan Digital Sky Survey (SDSS, York et al. 2000), to create a flux-limited sample of 174 sources, 90% of which have detections. Because the X-ray emission in radio-loud sources can have an additional component from the jet (e.g., Zamorani et al. 1981; Wilkes & Elvis 1987), we focus our analysis on the radio-quiet majority. We use these sources to perform a

multivariate analysis of α_{ox} , Γ_X , L_{UV} , and z in a manner that allows us to effectively separate the dependence of the X-ray spectral properties on L_{UV} and z .

We adopt a cosmology based on the the WMAP best-fit parameters ($h = 0.71$, $\Omega_m = 0.27$, $\Omega_\Lambda = 0.73$, Spergel et al. 2003). For ease of notation, we define $l_{UV} \equiv \log \nu L_\nu(2500\text{\AA})$, and $l_X \equiv \log \nu L_\nu(2 \text{ keV})$.

2. OBSERVATIONS AND COMPARISON SAMPLE

The new observations targeted seven non-BAL RQQs with $z > 4$ from the literature. These were known to be among the faintest ($\nu L_\nu(2500\text{\AA}) \lesssim 3 \times 10^{46}$ ergs s $^{-1}$) $z \sim 4$ optically-selected quasars to be observed thus far by *Chandra* or *XMM-Newton*. All seven were observed on-axis on the ACIS-S3 chip with exposure times 10–23 ksec. The exposure times were chosen in order to ensure that the X-ray source would be detected if $\alpha_{\text{ox}} < 1.9$. All targets were, in fact, detected. The new observations are summarized in Table 1.

The other $z \gtrsim 4$ sources were selected from the literature (Bechtold et al. 2003; Vignali et al. 2001, 2003a), and had been observed as targeted observations with *Chandra*. The $z \lesssim 4$ sources were found by cross-correlating the SDSS DR3 quasar catalogue (Schneider et al. 2005) with the *Chandra* public archive as of 2005 February 22. We selected those SDSS DR3 quasars that were serendipitously within 12' of a *Chandra* target. The radio-quiet sources were selected to have $R_i = 0.4(i - t_{1.4\text{GHz}}) < 1.5$ (Ivezić et al. 2004), where, $t_{1.4\text{GHz}}$ is the FIRST 1.4 GHz AB magnitude, and i is the SDSS i -band magnitude. The radio-loud sources were omitted because such sources have an additional component of X-ray emission arising from the jet (e.g., Wilkes & Elvis 1987; Worrall et al. 1987). Almost all of the $z < 4$ quasars have their *Chandra* data reported here for the first time.

The optical/UV spectra for each source were inspected by eye to exclude the BALs or any sources that had significant absorption. It is necessary to remove the BAL QSOs because their high column density gives them the appearance of being X-ray weak (e.g., Green et al. 2001; Gallagher et al. 2002, 2006), potentially biasing our analysis. We are unable to remove the high-ionization BAL quasars for $z < 1.5$, as their identification requires observations of the C IV line. We are able to remove low-ionization BALs at $0.45 < z < 2.25$ based on Mg II absorption. Reichard et al. (2003) found the fraction of BALs in the SDSS to be $\sim 14\%$, and therefore we expect there to be 13 ± 3 BALs in our sample at $z < 1.5$. We did not include seven sources with an obvious contribution in their spectra from the host-galaxy. Host-galaxy contamination is likely negligible for all included sources, except for possibly the lowest luminosity quasars, since $\nu L_\nu^* \sim 10^{44}$ ergs s $^{-1}$ at 2500\AA for galaxies (Budavári et al. 2005).

We visually inspected the *Chandra* events files to find those sources that fell on an ACIS chip. We did not include any sources that were observed on chip S4 due to higher read-out noise (Data Caveats on CIAO web pages ¹). All X-ray sources reported are within 1''–2'' of the optical position. The archival sources and their X-ray properties are listed in Table 2.

Altogether, the sample consists of 174 radio-quiet quasars, with a broad range in redshift ($0.1 < z < 4.7$) and luminosity (10^{44} ergs s $^{-1} \lesssim \nu L_\nu(2500\text{\AA}) \lesssim 10^{48}$ ergs s $^{-1}$). All sources have been observed with the *Chandra X-ray Observatory* using the ACIS-S or ACIS-I detectors, and 157 (90%) of them are detected. The (L_{UV}, z) distribution of the sample is shown in Figure 1.

¹<http://cxc.harvard.edu/ciao/caveats>

2.1. X-ray Spectra

Source extraction was done using *CIAO* 3.2.2² and *CALDB* 3.1. We extracted the PHA spectrum for all 174 sources using a circular aperture with radius chosen to include 95% of 3.5 keV photons. Typical extraction regions range from 5" for on-axis sources, to 10"–30" for most off-axis sources. The background was extracted from an annular region centered on the source, and any nearby sources were removed from the extraction regions. A correction for pileup was necessary for only one source in our sample, MRK 1014. The distribution of source counts is shown in Figure 2.

Spectral fitting was done using the *CIAO* tool *SHERPA* (Freeman et al. 2001). We estimated the parameters for a power law of the form

$$N(E) = n_0 \left(\frac{E}{1 \text{ keV}} \right)^{-\Gamma_X}, \quad (1)$$

where Γ_X is the photon index and n_0 is the normalization at 1 keV, in units of photons $\text{keV}^{-1} \text{ cm}^{-2} \text{ s}^{-1}$. We restricted our fits to energies 0.3–7.0 keV, and included Galactic absorption with N_H fixed to that inferred from 21 cm maps (COLDEN³ Dickey & Lockman 1990). If the source had < 200 counts, we fit the unbinned spectrum using the Cash statistic (Cash 1979). For these sources, the background was fit simultaneously with Equation (1) using an empirically determined background for the ACIS-S and ACIS-I, respectively. If the source had < 50 counts, we calculated n_0 by fixing $\Gamma_X = 1.9$, a typical value for RQQs (Reeves & Turner 2000; Piconcelli et al. 2003). We also estimate Γ_X for these sources, but fix $\Gamma_X = 1.9$ when calculating n_0 to stabilize the estimates of L_X and α_{ox} . We fit n_0 and Γ_X simultaneously for sources with counts between 50 and 200. If the source had > 200 counts, we fit the binned spectrum by minimizing χ^2 and included an intrinsic neutral absorber if justified by the data; only two of the sources with > 200 counts showed evidence for intrinsic absorption. These were 1438+0335 and 0958+0734, with intrinsic $N_H = 5.34^{+0.745}_{-0.203} \times 10^{21} \text{ cm}^{-2}$ and $N_H = 1.363^{+2.034}_{-0.626} \times 10^{22} \text{ cm}^{-2}$, respectively; the errors are at 95% confidence. The background for the > 200 count sources was binned and subtracted before spectral fitting. There were 86 sources with < 50 counts, 44 sources with between 50 and 200 counts, and 44 sources with > 200 counts.

We included an intrinsic neutral absorber for sources 0259+0048, 0918+5139, 1002+5542, and 1411+5205, despite the fact that they have < 200 counts. These sources initially exhibited unusually hard X-ray spectra ($\Gamma_X \lesssim 1$), so we fit Γ_X and N_H simultaneously to test if these low values of Γ_X were caused by unrecognized absorption. Even after including an absorber at the quasar redshift, sources 0259+0048, 0918+5139, and 1002+5542 still have rather hard X-ray continua, with photon indices of 1.02 ± 0.24 , 0.92 ± 0.33 , and 1.27 ± 0.15 , respectively. Such hard X-ray spectra could be the result of more complex absorption, such as an ionized or partial covering absorber. However, the low number of counts for these sources preclude obtaining meaningful spectral fits for more complex models. In addition, the mean Γ_X for our sample is ≈ 2 and the observed dispersion in Γ_X for our sample is 0.44. Thus, we might expect to observe a few sources with $\Gamma_X \sim 1$ in a sample with 157 X-ray detected sources, and therefore these three sources are probably not outliers but just represent the tail of the RQQ Γ_X distribution.

Source 1411+5205 shows evidence for considerable absorption, $N_H \sim 10^{23} \text{ cm}^{-2}$, and may be a BAL QSO. A 95% confidence interval on the column density for this source is $1.8 \times 10^{22} \text{ cm}^{-2} < N_H < 2.45 \times 10^{23} \text{ cm}^{-2}$.

²Chandra Interactive Analysis of Observations (CIAO), <http://cxc.harvard.edu/ciao/>

³For COLDEN, see <http://cxc.harvard.edu/toolkit/colden.jsp>

We used the projection method in *Sherpa* to estimate a 3σ confidence interval on n_0 . Those sources that did not contain $n_0 = 0$ in their 3σ confidence interval were considered detected, otherwise we set a 3σ upper limit on n_0 . For those sources with < 50 counts, the projection method was used to calculate the 68% (1σ) individual confidence intervals on the power law parameters. We calculated the covariance matrix of the parameters for those sources with > 50 counts.

Fifteen sources were in multiple observations. For each of these sources, all of the observations were fit simultaneously assuming the same power-law spectrum.

Based on our X-ray spectral fits, we estimate the mean value of Γ_X for our sample to be $\bar{\Gamma}_X = 2.033 \pm 0.034$, with an observed dispersion of 0.44. After accounting for the additional scatter in Γ_X caused by measurement error, we find that the intrinsic dispersion of Γ_X is ~ 0.31 . This is consistent with the dispersion found in other studies (e.g., Piconcelli et al. 2005; Brocksopp et al. 2006; Grupe et al. 2006). The intrinsic dispersion in Γ_X is similar to the intrinsic dispersion in the optical/UV spectral slope (Richards et al. 2001).

2.2. Optical/UV Spectra

Optical spectra were obtained for most sources from the SDSS. We also obtained spectra for some of the high redshift quasars from Anderson et al. (2001), Péroux et al. (2001), and Constantin et al. (2002).

We corrected the optical spectra for Galactic absorption using the $E(B-V)$ values taken from Schlegel et al. (1998), as listed in the NASA/IPAC Extragalactic Database (NED), and the extinction curve of Cardelli et al. (1989), assuming a value of $A_V/E(B-V) = 3.1$. We model the continuum as a power law of the form $f_\nu \propto \nu^{-\alpha}$, and the Fe emission as a scaled and broadened iron template extracted from I Zw I in the UV by Vestergaard & Wilkes (2001). The continuum and iron emission were fit simultaneously using the Levenberg-Marquardt method for nonlinear χ^2 -minimization. The continuum fitting windows are listed in Table 3. The median value of α for our sample is 0.602, and the dispersion in α is ≈ 0.4 .

We were not able to obtain a spectrum for Q 0910+564. For this source, we calculated the flux density at 2500\AA from the AB magnitude at $1450(1+z)\text{\AA}$ and the spectral index reported by (Schneider et al. 1991).

We were not able to use a power-law fit to calculate l_{UV} for the $z < 0.3$ sources, as the SDSS spectral range for these sources does not contain the rest-frame UV continuum. We therefore performed a linear regression of the dependence of l_{UV} on $\log \nu L_\nu(5100\text{\AA})$ and α_{opt} for higher redshift sources ($0.3 < z < 1.2$) for which we had all three quantities. Here α_{opt} is the spectral index of the optical continuum. Using the regression results, l_{UV} was then estimated for the $z < 0.3$ sources based on their optical luminosity and spectral index. The optical continuum parameters were found in the same manner as for the UV continuum, except that we used the Fe emission template from Véron-Cetty et al. (2004). For sources within $0.3 < z < 1.2$ the scatter about the regression fit resulted in a ‘measurement’ error on l_{UV} of ≈ 0.07 dex. For comparison, typical measurement errors on l_{UV} for the $z > 0.3$ sources are ≈ 0.001 – 0.01 dex, ignoring variability.

2.3. α_{ox}

We calculate the ratio of optical to X-ray flux (Tananbaum et al. 1979) as

$$\alpha_{\text{ox}} = -\frac{\log(f_X/f_{UV})}{\log(\nu_X/\nu_{UV})}, \quad (2)$$

where f_X and f_{UV} are the rest-frame flux densities at 2 keV and 2500Å, respectively. If the flux density from 2500Å to 2 keV is a simple power law, then α_{ox} is the spectral slope of this continuum, and thus α_{ox} may be thought of as a crude estimate of the shape of the ionizing continuum. The parameter α_{ox} is an important parameter for model comparison, as it summarizes the amount of energy emitted in the X-ray region (most likely a Comptonized component), compared with that emitted in the optical-UV (accretion disk component). The mean α_{ox} of our sample is $\bar{\alpha}_{\text{ox}} = 1.49 \pm 0.01$, and the dispersion of α_{ox} is estimated to be $\sigma_{\text{ox}} \approx 0.19$. Because some of the data points are censored, these estimates of the mean and dispersion of α_{ox} were obtained by maximum-likelihood assuming a normal density. The Kaplan-Meier estimate of the mean (e.g., Feigelson & Nelson 1985), a non-parametric estimate, gives $\bar{\alpha}_{\text{ox}} = 1.49 \pm 0.06$.

In Figure 3 we show the distributions of l_X and α_{ox} as functions of l_{UV} and z . We report the X-ray and UV parameters in Table 4.

3. DEPENDENCE OF α_{ox} ON L_{UV} AND z

3.1. Regression Results

In order to study the relationship between α_{ox} , optical/UV luminosity, and redshift, we performed a multivariate regression of α_{ox} on z and l_{UV} . In our analysis, we perform the regression using several different parameteric models for the redshift and l_{UV} dependencies. We compare the different models simultaneously using the Kullback-Leibler information (KLI; Kullback & Leibler 1951), a well-studied method for comparing data to models from information theory. In Appendix A, we describe KLI minimization in detail, and compare this approach to classical statistical methods for testing for significance.

Currently, there is no *a priori* reason to assume a certain parameteric form for a dependence α_{ox} on L_{UV} and z . Initially, we are interested in testing for the existence of a dependence of α_{ox} on redshift and on UV luminosity, and we are not concerned with the particular parameteric forms of the possible redshift and luminosity dependencies. As described in Appendix A, the KLI is a particularly powerful tool for comparing and testing several different parameteric models simultaneously, and is valid even if the ‘correct’ parameterization is not among those considered.

We compare models with redshift dependencies of the form $L_X \propto e^{-t(z)/t_0}$, $L_X \propto e^{z/z_0}$, and $L_X \propto (1+z)^{\beta\zeta}$, and L_{UV} dependencies of the form $L_X \propto L_{UV}^{\beta\iota}$. Here, $t(z)$ is the age of the universe at z in units of Gyr. In addition, Steffen et al. (2006) found some evidence for a nonlinear dependence of α_{ox} on l_{UV} , and to test this we include models that contain a quadratic term for l_{UV} .

We also tested for including the UV spectral slope, α_{UV} , as one of the independent variables. However, we found no evidence that α_{ox} depended on α_{UV} .

Each of the statistical models considered here may be expressed as a normal density with variance σ^2 and mean $E(\alpha_{\text{ox}}) = \bar{\alpha}_{\text{ox}}(\gamma)$. Here, $E(\alpha_{\text{ox}})$ is the expectation value of α_{ox} at a given l_{UV} and z , and γ denotes

the regression coefficients. The five models considered differ in their description of $\bar{\alpha}_{\text{ox}}(\gamma)$:

$$\mathcal{M}_z : \bar{\alpha}_{\text{ox}}(\gamma) = \gamma_0 + \gamma_l l_{UV} + \gamma_z z \quad (3)$$

$$\mathcal{M}_\zeta : \bar{\alpha}_{\text{ox}}(\gamma) = \gamma_0 + \gamma_l l_{UV} + \gamma_\zeta \log(1 + z) \quad (4)$$

$$\mathcal{M}_t : \bar{\alpha}_{\text{ox}}(\gamma) = \gamma_0 + \gamma_l l_{UV} + \gamma_t t(z) \quad (5)$$

$$\mathcal{M}_l : \bar{\alpha}_{\text{ox}}(\gamma) = \gamma_0 + \gamma_l l_{UV} + \gamma_{l^2} l_{UV}^2 \quad (6)$$

$$\mathcal{M}_{l+t} : \bar{\alpha}_{\text{ox}}(\gamma) = \gamma_0 + \gamma_l l_{UV} + \gamma_{l^2} l_{UV}^2 + \gamma_t t(z). \quad (7)$$

Here, we have introduced the notation that \mathcal{M}_z stands for the model that parameterizes the average value of α_{ox} as depending linearly on redshift, and similarly for the remaining four models. We do not include models with terms higher than quadratic in l_{UV} because such models were estimated to give a poorer fit to the data (cf. § 3.4). Model \mathcal{M}_t is almost identical to the parameterization used by several other authors (e.g., AT86, W94, S06), with the exception that other authors have used the fractional cosmological look-back time, $\tau(z) = 1 - t(z)/t(0)$.

Because some of the values of l_X are only upper limits, we employ the Expectation-Maximization (EM) algorithm (Dempster, Laird, & Rubin 1977; Aitken 1981) to calculate the maximum-likelihood solution for the regression parameters. These parameters are the regression coefficients, γ , and the intrinsic variance about the linear relationship, σ^2 . The likelihood functions for these five models are normal densities with means given by Equations (3)–(7). The regression is carried out directly on $\alpha_{\text{ox}} = 0.384(l_{UV} - l_X + 2.605)$ using computer routines coded by the authors.

The results of the regressions using the entire *Chandra* sample are

$$\bar{\alpha}_{\text{ox}} = (-5.148 \pm 1.293) + (0.147 \pm 0.029)l_{UV} - (0.014 \pm 0.018)z, \quad \sigma = 0.157 \quad (8)$$

$$\bar{\alpha}_{\text{ox}} = (-7.048 \pm 1.443) + (0.190 \pm 0.033)l_{UV} - (0.293 \pm 0.137) \log(1 + z), \quad \sigma = 0.155 \quad (9)$$

$$\bar{\alpha}_{\text{ox}} = (-8.816 \pm 1.473) + (0.223 \pm 0.031)l_{UV} + (3.061 \pm 0.890) \times 10^{-2}t(z), \quad \sigma = 0.151 \quad (10)$$

$$\bar{\alpha}_{\text{ox}} = (62.83 \pm 30.48) - (2.816 \pm 1.336)l_{UV} + (3.226 \pm 1.464) \times 10^{-2}l_{UV}^2, \quad \sigma = 0.155 \quad (11)$$

$$\bar{\alpha}_{\text{ox}} = (24.22 \pm 32.88) - (1.212 \pm 1.428)l_{UV} + (1.560 \pm 1.552) \times 10^{-2}l_{UV}^2 + \quad (12)$$

$$(2.684 \pm 0.965) \times 10^{-2}t(z), \quad \sigma = 0.151. \quad (13)$$

For all of these models, α_{ox} increases (becomes more X-ray quiet) with increasing luminosity and decreases (becomes more X-ray loud) with increasing redshift. The intrinsic scatter about the relationships is estimated to be $\sigma \sim 0.15$.

3.2. Evidence for low-redshift BAL QSOs in the Sample

The estimates for the regression parameters are derived via maximum-likelihood. However, the likelihood functions assume that the residuals are normally distributed. If this assumption is not true, then it may bias our results. To test the assumption of normality in the residuals, in Figure 4 we compare the cumulative distribution function (CDF) of the standardized residuals for \mathcal{M}_t with the standard normal. The standardized residuals are the residuals normalized by the intrinsic scatter. The CDFs for the other models were very similar. As can be seen, there is evidence for a violation of the assumption of normality. A Kolmogorov-Smirnov (KS) test confirmed this, finding a probability of ≈ 0.001 – 0.007 that the maximum difference between the CDFs of the standardized residuals for the models and the standard normal is greater

than that observed, assuming that the two distributions are the same. In addition, inspection of the residuals reveals that there are several sources that are significantly more X-ray quiet than would be expected from Equations (8)–(13), and are therefore outliers. These sources are all censored (i.e., not detected in the X-rays) and at $z < 1.5$. As noted in § 2, the high column density of BAL QSOs gives them the appearance of being X-ray weak. Furthermore, we are unable to remove BALs at $z < 1.5$. These two facts suggests that the regression outliers are BALs, as they are unusually X-ray weak and at $z < 1.5$.

To test the possibility that the $z < 1.5$ censored sources are dominated by BALs, and thus affecting our regression analysis, we removed these 10 sources and recalculated the regressions. Note that this number is consistent with the expected number of BALs in the $z < 1.5$ sample (cf., § 2). While this may remove some non-BALs from the $z < 1.5$ sample, it is unlikely that removing a few censored non-BALs from the fit will significantly affect the results, since these sources are not expected to be outliers and the regression is dominated by the detected sources. However, the BALs can have a non-negligible effect on the regression even if they are censored because they have an additional absorption component that contributes to the observed X-ray luminosity, and therefore are not expected to follow the functional form assumed by the regression and can be outliers. The existence of outliers has the effect of biasing the estimate of the intrinsic scatter upwards, inflating the uncertainties on the regression coefficients, and therefore reducing the statistical significance of the regression coefficients.

After removing the $z < 1.5$ censored data points, we were left with a sample of 164 sources, 157 (96%) of which are detected. Performing the regressions on this second sample, we find

$$\bar{\alpha}_{\text{ox}} = (-5.340 \pm 1.097) + (0.150 \pm 0.025)l_{UV} - (0.004 \pm 0.015)z, \sigma = 0.131 \quad (14)$$

$$\bar{\alpha}_{\text{ox}} = (-7.152 \pm 1.229) + (0.192 \pm 0.028)l_{UV} - (0.224 \pm 0.116) \log(1+z), \sigma = 0.129 \quad (15)$$

$$\bar{\alpha}_{\text{ox}} = (-9.273 \pm 1.241) + (0.233 \pm 0.026)l_{UV} + (2.870 \pm 0.750) \times 10^{-2}t(z), \sigma = 0.125 \quad (16)$$

$$\bar{\alpha}_{\text{ox}} = (74.61 \pm 25.17) - (3.349 \pm 1.103)l_{UV} + (3.827 \pm 1.208) \times 10^{-2}l_{UV}^2, \sigma = 0.127 \quad (17)$$

$$\bar{\alpha}_{\text{ox}} = (40.97 \pm 27.34) - (1.949 \pm 1.187)l_{UV} + (2.370 \pm 1.288) \times 10^{-2}l_{UV}^2 + \quad (18)$$

$$(2.263 \pm 0.813) \times 10^{-2}t(z), \sigma = 0.124 \quad (19)$$

The results are very similar to Equations (8)–(19), but the intrinsic scatter has decreased and the significance levels of the regression coefficients are in general higher. Note that Equations (16) and (19) are equivalent to the form $L_X \propto e^{-t(z)/t_0}$, where the e -folding time is $t_0 = 5.75^{+4.98}_{-1.83}$ (95% confidence) Gyr for \mathcal{M}_t and $t_0 = 7.25^{+14.4}_{-2.96}$ (95% confidence) Gyr for \mathcal{M}_{l+t} .

The CDF of the standardized residuals for Equation (16) is also shown in Figure 4. As can be seen, the residuals no longer show any evidence for a significant divergence from normality, suggesting that we have minimized BAL contamination by removing the $z < 1.5$ censored sources. A KS test also found that the empirical distribution of the standardized residuals for all parameterizations considered are not significantly different than the standard normal, having p -values of $p \sim 0.1$.

3.3. α_{ox} Depends on Both L_{UV} and z .

It is apparent from Equations (14)–(19) that there is statistically significant evidence for a dependence of α_{ox} on l_{UV} ($> 6\sigma$ significance). In addition, there is evidence from model \mathcal{M}_t that α_{ox} depends on cosmic time (3.8σ significance), and evidence from model \mathcal{M}_l that the $\alpha_{\text{ox}}-l_{UV}$ relationship is nonlinear (3.2σ significance). While the coefficients for both parameterizations imply that our data are inconsistent with

the simple form $\bar{\alpha}_{\text{ox}} = \gamma_0 + \gamma_1 l_{UV}$, it is unclear which parameterization is the preferred one. In particular, because there is a strong correlation between l_{UV} and z , it is possible that the $\alpha_{\text{ox}}-t(z)$ relationship is simply correcting for the nonlinearity in the $\alpha_{\text{ox}}-l_{UV}$ relationship, and is thus a spurious result. Because the models are not nested, (i.e. one is not merely a subset of the next), we cannot use classical statistical methods, such as the likelihood ratio or F -test, to compare their relative merits (e.g., Efron 1984; Freeman et al. 1999; Protassov et al. 2002). Instead, we adopt an approach that attempts to find the model that minimizes the ‘distance’ to the true probability density that gives rise to the observed data. We do this by finding the model that minimizes the Kullback-Leibler information (KLI; see Appendix A).

We use the Akaike Information Criterion (AIC , Akaike 1974) to estimate the difference in KLI between models. We estimate the difference in KLI between two models by multiplying their difference in AIC by $1/2$. Terms of order higher than l_{UV}^2 increased the AIC for models \mathcal{M}_l and \mathcal{M}_{l+t} , and were not included in the analysis. Denoting the maximum likelihood estimate of the model parameters as $\hat{\theta}$, and the estimated KLI as $H(\hat{\theta})$, we find $H(\hat{\theta}_z) - H(\hat{\theta}_{l+t}) = 7.599$, $H(\hat{\theta}_\zeta) - H(\hat{\theta}_{l+t}) = 5.798$, $H(\hat{\theta}_l) - H(\hat{\theta}_{l+t}) = 2.770$, and $H(\hat{\theta}_t) - H(\hat{\theta}_{l+t}) = 0.677$. Here, $H(\theta_z)$ denotes the KLI for model \mathcal{M}_z , and likewise for $H(\theta_\zeta)$, $H(\theta_l)$, $H(\theta_t)$, and $H(\theta_{l+t})$. Model \mathcal{M}_{l+t} is best supported by the empirical evidence.

Plots showing the residuals and partial residuals for the \mathcal{M}_{l+t} regression are shown in Figure 5. To visualize the result, Figure 6 shows a 3-dimensional plot of the best fit for this model. The partial residual plots display the dependence of α_{ox} on L_{UV} , after accounting for the dependence on cosmic time, and the dependence of α_{ox} on z , after accounting for the dependence on L_{UV} . Both of these figures correspond to the regression results after removing the suspected BALs. Also shown in Figure 5 are non-parametric fits to the residuals, calculated using a locally-weighted average based on a Gaussian smoothing kernel; the kernel width was chosen using generalized cross-validation (e.g., see Hastie, Tibshirani, & Friedman 2001). As can be seen, according to this model the nonlinearity in the $\alpha_{\text{ox}}-l_{UV}$ dependence, if real, is such that α_{ox} increases (becomes more X-ray quiet) faster at higher l_{UV} . This trend is in agreement with the results of Steffen et al. (2006), who found evidence that the slope of the $\alpha_{\text{ox}}-l_{UV}$ correlation may be steeper at higher l_{UV} .

Based on the AIC , model \mathcal{M}_{l+t} , which contains the $t(z)$ parameterization with a quadratic l_{UV} term, appears to provide the best description of our data, followed by the $t(z)$ parameterization with only a linear l_{UV} term.

3.4. Effects of Sampling and Nonlinear Dependence of α_{ox} on Luminosity

To assess how our estimate of the KLI varies under sampling from the underlying joint distribution of $(\alpha_{\text{ox}}, l_{UV}, z)$, we use the non-parametric bootstrap (Efron 1979). We drew 10^4 bootstrap samples and performed the regression for each parameterization on each bootstrap sample. We then estimated the KLI in the same manner, with the exception that we now use the sample mean of the difference in log-likelihoods of the *original* sample, evaluated at the maximum likelihood estimate of θ based on the bootstrapped samples. The sampling distributions of the differences in KLI between $\mathcal{M}_z, \mathcal{M}_\zeta, \mathcal{M}_l$, and \mathcal{M}_t , with respect to \mathcal{M}_{l+t} , are shown in Figure 7. The $t(z)$ parameterization with quadratic l_{UV} term, \mathcal{M}_{l+t} , had the smallest estimated KLI for $\approx 99.9\%$ of the bootstrap samples. Therefore, the preference for \mathcal{M}_{l+t} is unlikely to have resulted from fluctuations caused by random sampling, and thus it appears that this parameterization provides the best description of our data.

It is unlikely that the evidence for evolution is a result of nonlinearity in l_{UV} . Assuming that there is

no dependence of α_{ox} on z , we can use a suitably large enough polynomial expansion of l_{UV} to approximate any smooth nonlinear dependence of α_{ox} on l_{UV} . However, as mentioned above, model \mathcal{M}_l had the best *AIC* among the set of polynomial expansions in l_{UV} , and thus our data does not prefer terms of order higher than l_{UV}^2 . Therefore, \mathcal{M}_l should be viewed as the best approximation to the $\alpha_{\text{ox}}-l_{UV}$ relationship that is supported by our data without overfitting, and assuming that α_{ox} is independent of z . However, because the models that included $t(z)$ had an *AIC* lower than \mathcal{M}_l , and because \mathcal{M}_l had an *AIC* lower than models that included terms of higher order, it follows that models \mathcal{M}_{l+t} and \mathcal{M}_t are preferred by our data over any polynomial expansion of α_{ox} as a function of l_{UV} . This is not to say that models \mathcal{M}_{l+t} and \mathcal{M}_t are preferred over any smooth nonlinear function of l_{UV} , but that if such a function exists, it is unlikely to differ significantly from \mathcal{M}_l . The nonlinear effects are not extreme, and in fact are not ‘statistically significant’ in the classical sense. However, while there is not enough evidence in the data to reject a null hypothesis that α_{ox} is linear in l_{UV} and $t(z)$ at, say, $> 2\sigma$ significance, the empirical evidence supports a nonlinear dependence of α_{ox} on l_{UV} at a given z over a linear dependence.

3.5. Effect of Variability and Measurement Error on the Results

Measurement error or variability may induce false correlations between parameters. In this section, we consider two effects. The first is especially important when many sources are near the flux limit of the sample, and when the number of sources increases strongly with decreasing flux. In the second case, a bias can result even if all the sources are far above the flux limit.

For the first case, we argue that the expected tendency would be for α_{ox} to *increase* with increasing redshift, the opposite of what we claim from the data. Consider the possibility that the sources are variable. Assume for simplicity of argument that the sources vary around some mean flux in all spectral bands, and that a particular source spends an equal amount of time brighter than the mean and dimmer than the mean. Then the sources that were discovered by SDSS near the flux limit are preferentially observed in their ‘bright’ state. By the time we observed them with Chandra, they will likely no longer be in their ‘bright’ state, and thus may be systematically X-ray quieter. Thus we expect the sources near the flux limit to appear fainter in X-rays on average than they really are. Since most of the sources near the flux limit are at high redshift, the tendency may be for α_{ox} to increase (quasars are less X-ray bright) with redshift. Since this is the opposite of what we see, variability of sources near the flux limit is not producing the result.

For measurement error, the qualitative argument is similar. Near the flux limit, random errors in photon counts result in more sources just below the limit being randomly included in the sample than sources above the limit being randomly excluded, provided that the number of sources is an increasing function of decreasing flux limit (which is the case here). Thus, the SDSS selection would again be biased towards sources with optical fluxes that appear brighter in optical than they really are. Chandra then measured X-ray fluxes for essentially all the sources. Thus, we expect the sources near the flux limit to be systematically more X-ray faint than they really are. Again, this is the opposite of what we see in the data, so this Malmquist-type bias is not important.

For the second case, measurement errors or variability may induce false correlations even if all sources are detected far above the flux limit. However in this case, Monte Carlo simulations can be carried out to see how important the effect might be. Measurement errors on the independent variables can bias the estimates of the regression coefficients (e.g., Akritas & Bershady 1996; Fox 1997), and errors on the dependent variable can bias the coefficient estimates for censored regression. When the dependent variable is measured

with error and/or variability, the measurement error and variability inflate the observed variance in the regression residuals, biasing the estimate of the intrinsic scatter, σ^2 . For ordinary least-squares this is not a problem, since the estimate for the intrinsic scatter, σ^2 , and the estimates of the regression coefficients, γ , are statistically independent. However, for the censored regression model, the estimates of the intrinsic scatter and the coefficients are no longer statistically independent, and the bias in the intrinsic scatter estimate also carries over to the coefficient estimates (Stapleton & Young 1984). These facts are confirmed by Monte Carlo simulations, which have shown that the *observed* relationship between l_X and l_{UV} can differ from the intrinsic relationship when the observed l_X and l_{UV} differ significantly from the intrinsic l_X and l_{UV} (e.g., Yuan et al. 1998b). Since the UV and X-ray data are measured with error, we are not fitting the intrinsic distribution of l_X given l_{UV} and z , but rather the distribution of $l_X + \epsilon_X$ at a given $l_{UV} + \epsilon_{UV}$ and z , where ϵ_X and ϵ_{UV} are random error terms. The errors for l_{UV} are the usual measurement errors from the continuum fitting and are very small in our analysis, with typical values of $\sigma_{UV} \approx 0.001$ – 0.01 dex. However, the errors for l_X include the contribution from measurement errors and from variability. The errors from variability of the X-ray emission arise from the fact that the X-ray and optical observations are not simultaneous. We are interested in the distribution of l_X at a given l_{UV} and z ; however, because the X-ray observations are not simultaneous with the optical, we do not observe the value of l_X given l_{UV} for each source, but some value of l_X which has varied from the original X-ray luminosity at the time of the optical observations.

Typical long-term X-ray variability for Seyfert 1s is 20%–40% with no obvious trend with luminosity (Grupe et al. 2001; Uttley et al. 2002; Markowitz et al. 2003). The measurement errors in l_X for our sample are typically ~ 0.07 dex. Assuming X-ray variability amplitudes of 30% for the sources in our sample, this implies typical uncertainties in the X-ray luminosity of ~ 0.15 dex. Correcting the scatter in α_{ox} for the contribution from X-ray variability and measurement error, we find an implied intrinsic scatter in l_X of $\sigma \approx 0.29$ dex.

To assess whether the observed dependence of α_{ox} on z is the result of bias arising from variability, we performed Monte Carlo simulations. Because we are interested in testing if a spurious redshift dependence may occur due to this type of bias, we simulate values of l_X , given l_{UV} , assuming $L_X \propto L_{UV}^{0.65}$. Within the framework of model \mathcal{M}_t , this form corresponds to assuming $\gamma_l = 0.134$ and $\gamma_t = 0$, and therefore α_{ox} depends only on UV luminosity for these simulations. The value of $\beta_l = 0.65$ was chosen because a linear regression of l_X on l_{UV} found $L_X \propto L_{UV}^{0.631 \pm 0.088}$, consistent with the work of Avni & Tananbaum (1986), Wilkes et al. (1994), Vignali et al. (2003b), Strateva et al. (2005), and Steffen et al. (2006).

The simulations were performed as follows. We first drew 164 values of l_{UV} and $t(z)$ from a kernel estimate of their joint distribution (Silverman 1986), after removing the censored $z < 1.5$ sources. Then, we calculated values of l_X , assuming $L_X \propto L_{UV}^{0.65}$. The random Gaussian scatter in l_X about the l_{UV} dependence had a standard deviation of $\sigma = 0.30$ dex; this value was motivated by the regression results. To simulate the upper limits, we randomly censored 6 of the values of l_X , and increased their censored values by a small random amount. We added random Gaussian noise to the uncensored values of l_X to simulate the effects of variability and measurement error, where the standard deviation of this noise was 0.15 dex. To simulate the effect of the measurement errors on l_{UV} , we also added random Gaussian noise of standard deviation 0.005 dex to the values of l_{UV} . We then performed censored regression on the simulated values. We repeated this procedure for 10^4 simulations, and calculated the average simulated regression coefficients for model \mathcal{M}_t , $\bar{\gamma} = (\bar{\gamma}_l, \bar{\gamma}_t)$, and their covariance matrix, Σ_γ .

We calculate the χ^2 of our regression coefficients for \mathcal{M}_t estimated from our sample, $\hat{\gamma} = (0.233, 0.029)$, as $\chi^2_2 = (\hat{\gamma} - \bar{\gamma})^T \Sigma_\gamma^{-1} (\hat{\gamma} - \bar{\gamma})$. Here, x^T is the transpose of x . We found a value of $\chi^2_2 = 11.62$; under the null hypothesis that $\gamma_l = 0.134$ and $\gamma_t = 0$, the probability of observing a χ^2_2 this high or higher

is $\lesssim 3 \times 10^{-3}$. Similar results were found by calculating the χ^2 of the regression coefficients for \mathcal{M}_{l+t} . Therefore, our observed values of γ_t are highly unlikely to be a spurious correlation resulting from variability and measurement error.

In summary, we argue that Malmquist-type biases from measurement error or variability will induce a false correlation of α_{ox} with z in the *opposite* sense of what is observed, and therefore are not causing our finding. We further showed through simulations that measurement errors or variability for objects within the sample are likewise not capable of inducing a false correlation between variables.

3.6. Rank Correlation Analysis

An alternative test for evolution of the X-ray emission for a given UV luminosity is Kendall’s generalized partial τ (Akritas & Siebert 1996). Kendall’s partial τ has been used by Vignali et al. (2003b), Strateva et al. (2005), and Steffen et al. (2006), where they did not find any evidence for a partial correlation between α_{ox} and z based on it, consistent with their parametric analysis. However, Kendall’s partial τ has some undesirable properties that make it difficult to assess the statistical significance of the result (Nelson & Yang 1988). In particular, conditional independence between variables 1 and 2, given a third variable, does *not* necessarily correspond to a value of $\tau = 0$. Alternatively, conditional dependence of two variables given a third does not necessarily correspond to a value of $\tau \neq 0$. Within the context of this work, this implies that a value of $\tau = 0$ does not necessarily correspond to the null hypothesis that α_{ox} (or L_X) is independent of z at a given L_{UV} ; i.e., an expected value of $\tau = 0$ does not necessarily result when $p(L_X|L_{UV}, z) = p(L_X|L_{UV})$.

In order to test the reliability of Kendall’s partial τ , we use Monte Carlo simulations to compare the distributions of τ under the assumption that α_{ox} only depends on L_{UV} , and under the assumption that α_{ox} depends on both L_{UV} and z . For each of the simulations, we calculated values of Kendall’s partial τ for α_{ox} with z , $\tau_{\alpha z, l}$, and L_X with z , $\tau_{xz, l}$, controlling for the correlation between L_{UV} and z . We did this for two hypotheses. The ‘null’ hypothesis, H_0 , assumed $L_X \propto L_{UV}^{0.65}$, and the alternative (i.e., ‘evolution’) hypothesis, H_1 , assumed $L_X \propto L_{UV}^{0.40} e^{-t(z)/5.5}$. The simulations under both hypothesis were performed in the same manner as described in § 3.5. The results are shown in Figure 8.

Under the null hypothesis of no evolution, the expected values of τ for both L_X and α_{ox} are indeed non-zero. Using the sample average of the simulations as an estimate of the expectation values, we find that the expected value of $\tau_{\alpha z, l}$ under the assumption that α_{ox} does not depend on z is 0.105. However, under the assumption that α_{ox} does depend on z , the average simulated value of τ is -0.001. Surprisingly, the expected value of τ for the $\alpha_{\text{ox}}-z$ partial correlation is approximately equal to zero when α_{ox} depends on z , at least for the simulation performed here. We investigate the behavior of Kendall’s partial τ further in Appendix B.

For our quasar sample, we find a value of Kendall’s partial τ for L_X and z of $\tau_{xz, l} = 0.212$, and for α_{ox} and z of $\tau_{\alpha z, l} = 0.057$. Our sample has a value of Kendall’s regular τ between L_{UV} and z of $\tau_z = 0.686$. As can be seen from the distributions of the simulated τ , both of our observed values of τ are about as equally consistent with evolution of the X-ray emission at a given L_{UV} as with no evolution. In fact, there is considerable overlap between the distributions of τ under both hypotheses, thus making it difficult to distinguish between the two. Unfortunately, we are not able to decide in favor of either hypothesis using Kendall’s generalized partial τ .

Based on the simulations, the lack of evidence for a significant correlation between α_{ox} and z based

on Kendall’s generalized partial τ (Vignali et al. 2003b; Strateva et al. 2005; Steffen et al. 2006) may be the result of an incorrect assumption about the distribution of τ under the null hypothesis. However, it should be noted that the parametric tests performed by Vignali et al. (2003b), Strateva et al. (2005), and Steffen et al. (2006) also did not reveal any evidence for evolution of α_{ox} . In addition, although we have shown that one can both incorrectly reject and accept the null hypothesis based on the partial τ statistic, there has never been a claimed rejection of the null hypothesis of no evolution in α_{ox} in previous studies.

4. RESULTS FOR Γ_X

To investigate any dependence of the X-ray photon index, Γ_X , on UV luminosity and redshift, we performed a weighted linear regression of Γ_X on l_{UV} and $\log(1+z)$ using all 157 detected sources. The weights are made up of a combination of the intrinsic scatter in Γ_X and the measurement errors on Γ_X . The results are

$$\Gamma_X = -3.43(\pm 3.879) + 0.125(\pm 0.087)l_{UV} - 0.678(\pm 0.347)\log(1+z). \quad (20)$$

Based on this regression, there is no significant evidence for a dependence of Γ_X on L_{UV} or z , although the z dependence is marginally significant at $\approx 2\sigma$.

Similar to α_{ox} , we experimented with parameterizing the z dependence using $t(z)$ and z . There was no noticeable difference between the different parameterizations, although the $\log(1+z)$ model gave slightly better results in the sense of minimizing mean squared error. In addition, if any z dependence of Γ_X is due to a systematic hardening of the X-ray spectra at higher energies, then we might expect the z dependence to be best parameterized using $\log(1+z)$.

We show the joint confidence regions of the l_{UV} and $\log(1+z)$ coefficients in Figure 10. While there is no significant evidence that Γ_X is related to either L_{UV} or z , we note that the measurement errors on Γ_X are large and contribute significantly to enlarging the confidence region of the regression coefficients. Because the confidence region of the regression coefficients is large, the possibility that Γ_X is significantly correlated with both UV luminosity and redshift is also consistent with our data.

Previous work by Gallagher et al. (2005) has found evidence for an anti-correlation between Γ_X and α_{UV} . Motivated by their work, we also perform a linear regression of Γ_X on α_{UV} . We only included those $z > 0.5$ sources detected by Chandra, leaving us with 136 sources. The redshift limit was imposed to ensure that an adequate amount of the UV continuum was available for estimating α_{UV} . We used the *FITEXY* procedure (Press et al. 1992) with the Tremaine et al. (2002) modification to account for the measurement errors in both Γ_X and α_{UV} , and the intrinsic scatter about the regression. The result of the regression is:

$$\Gamma_X = 2.21(\pm 0.07) - 0.25(\pm 0.07)\alpha_{uv}. \quad (21)$$

The α_{UV} coefficient is significant at 3.5σ . The regression results are consistent with the assumption that Γ_X is linearly related to α_{UV} , and the residuals are approximately normally distributed. We also performed a Spearman and Kendall rank correlation test between the two spectral slopes, and found an anti-correlation of similar significance.

To test if including the UV red quasars affect our limits on the luminosity and redshift dependencies, we also performed the regression after removing all sources with $\alpha_{UV} > 1.2$. Removing these UV red quasars did not significantly change the confidence regions shown in Figure 10.

5. COMPARISON WITH PREVIOUS STUDIES OF α_{ox} .

The parametric dependence of α_{ox} on L_{UV} and z has been studied previously by several authors (e.g., Avni & Tananbaum 1982, 1986; Wilkes et al. 1994; Bechtold et al. 2003; Vignali et al. 2003b; Strateva et al. 2005; Steffen et al. 2006). In this analysis, we confirm the anti-correlation between α_{ox} and L_{UV} seen previously, but also find evidence for a correlation between α_{ox} and redshift. Most previous studies have not found any significant evidence that α_{ox} is related to z , with the exception of Bechtold et al. (2003). Yuan et al. (1998a) found evidence for a slight dependence of α_{ox} with z for $z < 0.5$, but with opposite sign as that found here. Using high-quality *Chandra* data, we find that α_{ox} is related to both L_{UV} and z .

We perform a quantitative comparison between our results and those of Avni & Tananbaum (1986), Wilkes et al. (1994), Strateva et al. (2005), and Steffen et al. (2006). These authors have presented their results using a different parameterization for evolution, where they have fit a linear relationship of the form⁴

$$\alpha_{\text{ox}} = A_l(l_{UV} - 30.5 - \log \nu_{UV}) + A_\tau(\tau(z) - 0.5) + A. \quad (22)$$

Here, $\tau(z)$ is the cosmological look-back time in units of the present age of the universe, and ν_{UV} is the frequency corresponding to 2500\AA . We fit a relationship of this form and find $A_l = 0.233 \pm 0.026$ and $A_\tau = -0.392 \pm 0.103$, with a correlation of $\text{Corr}(A_l, A_\tau) = -0.878$. In Figure 9 we show the 95% joint confidence region on our estimate of (A_l, A_τ) , as well as the 95% confidence ellipses for AT86, W94, S05, and S06. These authors do not report equations for their confidence regions, so we matched them by eye. We compare with the results of AT86 obtained using their entire sample, i.e., their BQS+BF+HET85 sample, and the results of W94 obtained using only the radio-quiet sources and assuming $\Gamma_X = 2$ as displayed in their Figure 14a. The results for the S05 sample are presented by S06.

Statistically, our results differ from the analysis of AT86 at the $\approx 4\sigma$ level, from W94 at the $\approx 2\sigma$ level, from S05 at the $\approx 2.5\sigma$ level, and from S06 at the $\approx 3\sigma$ level. However, there are a number of systematic differences between our analysis and those of AT86, W94, S05, and S06, that, when taken into account, may introduce an additional systematic component to the errors. The AT86 sample includes both radio-quiet and radio-loud sources, and as noted in § 2, the radio-loud sources can have an additional component in their X-ray emission from the jet. To avoid this type of contamination, we have only included RQQs in our sample. In addition, AT86 assumed a value of $\Gamma_X = 1.5$ when calculating the 2 keV flux. As has been found here and in many other studies, a value of $\Gamma_X \approx 2$ is more typical for RQQs. Wilkes et al. (1994) calculated A_τ for both $\Gamma_X = 1.5$ and $\Gamma_X = 2$ and found that assuming $\Gamma_X = 2$ had the effect of shifting A_τ towards more negative values. If the assumption on Γ_X affects the estimated A_τ for AT86 in the same way as for W94, then one would expect assuming $\Gamma_X = 2$ would shift the AT86 confidence ellipse toward our estimate.

The largest systematic difference between our work and that of AT86, W94, S05, and S06 is in the differing levels of heterogeneity of the samples and the different instruments used to collect the X-ray data. The AT86 and W94 X-ray observations were done using the *Einstein* Observatory Imaging Proportional Counter (IPC). About two-thirds of the X-ray data for the S06 sample was observed using the *ROSAT* Position Sensitive Proportional Counter (PSPC), with the remaining X-ray data from *Chandra* or *XMM-Newton*. S06 combined sources from the SDSS, COMBO-17 survey (Wolf et al. 2004), Bright Quasar Survey (Schmidt & Green 1983), a heterogeneous low- z Seyfert 1 sample, and a heterogeneous high- z sample similar to our high- z sample. The S06 sample is more heterogeneous than ours, but probes a wider range in luminosity; the ranges in cosmic age probed by S06 and our sample are very similar. The S05 sample is a

⁴The term $\log \nu_{UV}$ arises because we define l_{UV} to be the logarithm of $\nu_{UV}L_{UV}$

subset of the S06 sample, and does not contain the COMBO-17 and BQS sources. The main SDSS sample of S05 and S06 consists of 155 radio-quiet quasars that were selected from the SDSS and contained within the inner 19' of *ROSAT* PSPC pointings with exposure times > 11 ksec. Thus, the S05 sample is very similar to ours in its heterogeneity, with the exception of the additional low redshift Seyfert 1 sample; S05 perform their analysis both with and without the Seyfert 1 sample. The AT86 and W94 samples are both more heterogeneous than the S06 sample. In addition, the redshift ranges probed by the AT86 and W94 samples are smaller ($z < 3.3$) than that of the S06 sample, the S05 sample, and our sample, probing a slightly smaller range in cosmic time.

Our sample only consists of *Chandra* ACIS observations. Increased sensitivity gives *Chandra* the ability to detect sources with rest-frame 2–10 keV flux down to $f_{HB} \sim 2 \times 10^{-15}$ ergs s^{-1} in a ~ 20 ksec observation. In this work, we estimate the *Chandra* 2 keV flux densities using data over a broader spectral range (0.3–7 keV) than that probed by the *Einstein* IPC (0.4–4 keV) and the *ROSAT* PSPC (0.1–2.5 keV). Our sample is also more homogeneous than those used previously, except for the S05 SDSS + high- z sample, being made up almost entirely of SDSS sources which had serendipitous *Chandra* observations; unfortunately this also results in our sample probing a smaller range in luminosity. Similar to our work, the high- z samples of S06 and S05 both consist of sources with *Chandra* and *XMM* data, and the COMBO-17 sample of S06 also consists of *Chandra* data; both the S05 and S06 samples have slightly lower X-ray detection fractions than our sample.

Avni & Tananbaum (1986) and W94 estimate the 2500Å flux density from published B - and V -band magnitudes assuming a constant spectral slope of $\alpha = 0.5$. The 2500Å flux density for many of the S05 and S06 sources were measured directly from the SDSS spectra. However, the 2500Å flux densities for the 52 COMBO-17 sources of S06 were estimated by interpolation and extrapolation. The 2500Å flux densities for the 46 BQS sources in S06 were estimated from the 3000Å flux assuming a constant spectral slope of $\alpha = 0.5$. The dispersion in quasar spectral slopes is large (≈ 0.3 , Richards et al. 2001), and this large dispersion can result in a non-negligible error on l_{UV} if one assumes a constant spectra slope, especially if one is extrapolating over a large range in wavelength. These issues are exacerbated when one fits α_{ox} instead of l_X , as the errors on l_{UV} contribute to the errors on α_{ox} , thus not only increasing the scatter about the regression, but also correlating the errors on l_{UV} and α_{ox} . In addition, as noted in § 3.5, the X-ray variability can also bias the coefficients for censored regression. In particular, these issues will affect the AT84 and W94 results because of the larger wavelength difference between 2500Å and the B - and V -bands for many of the sources, and the lower detection fraction ($\sim 60\%$). The analysis of S05 and S06 is unlikely to be significantly affected by these issues due to the high detection fraction and large number of sources with directly measured 2500Å flux densities. Furthermore, these authors found consistent results when analyzing different subsamples of their data.

Strateva et al. (2005) report values of Kendall’s generalized partial τ for a partial correlation between α_{ox} and z , given L_{UV} , for their main SDSS sample combined with their high- z sample. Because the main + high- z sample of S05 is very similar to ours in distribution of L_{UV} and z and the number of sources, we expect that the distribution of Kendall’s partial τ under the no-evolution and evolution hypotheses should also be similar. Strateva et al. (2005) find a value of $\tau = 0.03$, where we have corrected for the sign difference between our definition of α_{ox} and theirs. This value of τ is consistent with our value of $\tau = 0.057$. Because their value of τ is not significantly different than $\tau = 0$, and because their parametric analysis gave similar results, S05 concluded that there is no evidence that α_{ox} changes with redshift. However, as per the discussion in § 3.6, the expected value of τ under the null hypothesis of no evolution in α_{ox} is in general not $\tau = 0$, and therefore it is inappropriate to calculate significance levels with respect to $\tau = 0$. Comparison with Figure 8

implies that the value of $\tau = 0.03$ found by S05 is about as equally consistent with the evolution hypothesis as with the no-evolution hypothesis. However, the parametric analysis by S05 still differs from ours at the $\approx 2.5\sigma$ level.

Similar to Bechtold et al. (2003), we find that α_{ox} is correlated with both UV luminosity and redshift. However, in contrast to Bechtold et al. (2003), we find that α_{ox} depends more strongly on L_{UV} than on z . In addition, we find that RQQs are systematically more X-ray loud at higher redshift. Bechtold et al. (2003) found that α_{ox} is larger (more X-ray quiet) for high- z sources, but found an overall trend where α_{ox} becomes more X-ray loud as z increases. Bechtold et al. (2003) did not perform a regression or partial correlation analysis, but we note that their observed marginal distribution of $\alpha_{\text{ox}}-z$ is such that α_{ox} becomes more X-ray loud as z increases for $z \lesssim 2$. This is opposite the trend seen in our data, where inspection of Figure 3 reveals that α_{ox} is observed to become more X-ray quiet with increasing z , if one does not correct for the $L_{UV}-z$ correlation.

The source of this discrepancy is likely the values of Γ_X used by Bechtold et al. (2003) for their *ROSAT* sources. Bechtold et al. (2003) used Γ_X values taken from Yuan et al. (1998a), which were calculated using the two hardness ratios given by the Standard Analysis Software System (SASS), to estimate the flux density at 2 keV. These values of Γ_X steadily decrease from $\Gamma_X \sim 2.6$ at $z \sim 0$, to $\Gamma_X \sim 2$ at $z \sim 2$. However, values of $\Gamma_X \sim 2.6$ are steeper than is commonly seen in RQQs, as has been found in this work and in other recent studies (e.g., Reeves & Turner 2000; Piconcelli et al. 2003). Therefore, assuming a power-law and the values of Γ_X obtained by Yuan et al. (1998a) may not provide an accurate estimate of the 2 keV flux density, and thus α_{ox} . If $\Gamma_X \sim 2$, then assuming values of $\Gamma_X \sim 2.6$ will systematically under-predict the 2 keV flux density for a given 0.1–2.4 keV flux, and consequently provide estimates of α_{ox} that are too large. Furthermore, a steady decrease from $\Gamma_X \sim 2.6$ at $z \sim 0$ to $\Gamma_X \sim 2$ at $z \sim 2$ would produce a similar observed decrease in α_{ox} from $z \sim 0$ to $z \sim 2$, thus increasing the magnitude of any $\alpha_{\text{ox}}-z$ anti-correlation. Considering that L_{UV} also increases with increasing z due to flux limits, this would also weaken any observed correlation between α_{ox} and l_{UV} , and thus lead Bechtold et al. (2003) to conclude that α_{ox} is a stronger function of redshift. This is what is observed in the Bechtold et al. (2003) data, where α_{ox} is observed to decrease from $z \sim 0$ to $z \sim 2$. At $z \sim 2$, the Yuan et al. (1998a) sources have values of Γ_X that are more typical of RQQs, $\Gamma_X \sim 2$. In addition, after $z \sim 2$, the trend in α_{ox} is observed to change sign, increasing with increasing z , consistent with the data presented here. This is also the redshift where the Bechtold et al. (2003) sample becomes dominated by *Chandra* sources, and have 2 keV flux densities calculated assuming $\Gamma_X = 2.2$.

6. DISCUSSION

In this paper we were able to separate the dependence of α_{ox} on the quasar luminosity, L_{UV} , from that of cosmic epoch, z , and we find that both dependencies are present, though with opposite sign. From this, it follows that RQQs become more X-ray quiet (increasing α_{ox}) with increasing UV luminosity, and become more X-ray loud with increasing redshift. An analysis based on the Kullback-Leibler information finds evidence that α_{ox} may depend nonlinearly on l_{UV} at a given $t(z)$, with α_{ox} increasing more rapidly as l_{UV} increases.

One may be able to find a better parameterization for the redshift dependence than the one adopted here, but that would only strengthen our claims of evidence for a dependence of α_{ox} on z . In addition, as argued in § 3.4, it is unlikely that the observed redshift dependence can be explained by nonlinearity in

the $\alpha_{\text{ox}}-l_{UV}$ relationship. However, expanding the model space to include other parameters such as black hole mass or accretion rate may provide a better fit and be preferred over models which contain only a redshift and L_{UV} dependence. For example, a dependence of α_{ox} on black hole mass, M_{BH} , is predicted by some models for accretion disk and hot corona (e.g., Janiuk & Czerny 2000; Bechtold et al. 2003). If such a correlation exists, then it may be that the $\alpha_{\text{ox}}-t(z)$ relationship is simply tracing the underlying evolution of the active black hole mass function, which is then projected onto the $\alpha_{\text{ox}}-t(z)$ plane via an $\alpha_{\text{ox}}-M_{BH}$ relationship. In this case the statistical model that contains M_{BH} would provide the best fit, and there would be no need for an additional redshift dependence. However, in the absence of such information, we find that the model that best describes our data is given in terms of a quadratic dependence on l_{UV} and a linear dependence on $t(z)$.

6.1. K -Corrections and the $\alpha_{\text{ox}}-z$ Relationship

It may be suggested that the α_{ox} dependence on z is caused by a varying Γ_X as the observed *Chandra* spectral range shifts to harder rest-frame energies. If Γ_X were to steepen at higher energies, creating a softer X-ray continuum at these energies, then we would be systematically over-estimating the 2 keV flux densities, thus explaining the $\alpha_{\text{ox}}-z$ relationship. While we do not find any strong evidence for a change in Γ_X with z , the results from § 4 shown in Figure 10 suggest that if there is spectral curvature, then Γ_X likely flattens with increasing energy. A flattening of the X-ray continua at higher energies is opposite the trend needed to explain the $\alpha_{\text{ox}}-z$ relationship, and thus our result cannot be explained by a systematic steepening of the intrinsic X-ray continuum at harder energies.

Because we do not fit an intrinsic absorber to most of our sources, it may also be suggested that the observed redshift dependence of α_{ox} is caused by redshifting of soft X-ray absorption out of the observed spectral region. An intrinsic absorber will more strongly absorb the softer X-rays, and therefore will more significantly affect the observed X-ray continuum of lower redshift sources. This could then cause a spurious anti-correlation between L_X and $t(z)$.

To test if the observed dependence of α_{ox} on $t(z)$ is the result of soft X-ray absorption shifting out of the observed band, we used *SHERPA*'s FAKEIT routine to simulate observed X-ray spectra as a function of z . We assumed a power-law continuum with $\Gamma_X = 2$, and an intrinsic neutral absorber with column density $N_H = 10^{21} \text{ cm}^{-2}$. We argue in the next paragraph that a column density of $N_H = 10^{21} \text{ cm}^{-2}$ is greater than the maximum N_H allowed by the Γ_X-z regression, and thus we use $N_H = 10^{21}$ as an upper limit on the effect of unrecognized neutral intrinsic absorption on the $\alpha_{\text{ox}}-z$ relationship. The observed X-ray continuum was simulated for a source at $z = 0, 1, 2, 3$, and 4, and the intrinsic luminosity of the source was kept constant. We then fit each simulated spectrum with only a power-law. This resulted in the inferred X-ray luminosity of $z = 0$ sources being a factor of ~ 2 lower than the $z = 4$ sources. Therefore, based on these simulations, ignoring intrinsic absorption can result in a spurious decline in L_X from $z = 4$ to $z = 0$ by a factor of ~ 2 when $N_H \sim 10^{21} \text{ cm}^{-2}$. However, the results of our α_{ox} regression imply that the X-ray luminosity drops by a factor of ~ 8 from $z = 4$ to $z = 0$, and therefore the observed $\alpha_{\text{ox}}-z$ relationship cannot be explained as a spurious correlation resulting from unidentified intrinsic neutral absorption.

We can use our simulated spectra to constrain a typical value of N_H for our sources, assuming that N_H remains roughly constant with redshift. The observed photon index of the simulated spectra dropped from $\Gamma_X = 2$ at $z = 4$ to $\Gamma_X \approx 1.4$ at $z = 0$. From Figure 10, we note that the 3σ limit on the maximal drop in observed Γ_X between $z = 4$ and $z = 0$ is $\Delta\Gamma_X \approx 0.35$. This is considerable less than the observed drop in

Γ_X from the simulations, and thus represents more than the maximal amount of change in Γ_X with redshift that is allowed by our data. Therefore, assuming only neutral absorption, values of $N_H \gtrsim 10^{21} \text{ cm}^{-2}$ would produce observed values of Γ_X at $z = 0$ that are too flat, and thus $N_H \lesssim 10^{21} \text{ cm}^{-2}$ for most of our sources.

Because the redshift dependence of α_{ox} cannot be explained by a systematic steepening of Γ_X at higher energies, or by an unidentified intrinsic neutral absorber shifting out of the observed *Chandra* bandpass, we conclude that the $\alpha_{\text{ox}}-z$ relationship is likely the result of evolution of the accretion mechanism and environment. However, more complex absorption models, such as an ionized or partial covering absorber cannot be ruled out as causing the observed $\alpha_{\text{ox}}-z$ dependence, but investigation of such models is beyond the scope of this work.

6.2. Γ_X Relationships

We do not find significant evidence for a correlation between the radio-quiet quasar X-ray spectral photon index, Γ_X , and UV luminosity or redshift. This is consistent with results obtained using *XMM* observations of SDSS RQQs (Risaliti & Elvis 2005), *ASCA* observations of RQQs (Reeves & Turner 2000), and fitting of composite spectra of $z > 4$ RQQs (e.g., Vignali et al. 2003c, 2005; Shemmer et al. 2006). However, this is in contrast with the work of Dai et al. (2004) and Bechtold et al. (2003). Dai et al. (2004), found evidence for a correlation between Γ_X and L_X using a small sample of gravitationally-lensed RQQs. Bechtold et al. (2003) used Kendall’s generalized τ to assess the 2-dimensional correlations between Γ_X and both luminosity and z , and found evidence that Γ_X is correlated with luminosity and anti-correlated with z . In this work we have used linear regression to control for the artificial correlation between luminosity and redshift, and find that there is no significant evidence that Γ_X varies with l_{UV} and z . However, inspection of Figure 10 reveals that if Γ_X does depend on l_{UV} and z , then the directions of these trends are likely in agreement with the correlations seen by Bechtold et al. (2003). In addition, a systematic flattening of Γ_X with increasing z has also been seen in *XMM* data by Page et al. (2003), and Vignali et al. (1999) found some evidence that Γ_X is flatter on average for $z \sim 2$ RQQs than for lower z RQQs..

It is interesting to note that at $z \sim 2$ the observed *ROSAT* band has shifted to $\sim 0.3-7.2$ keV in the quasar rest-frame, overlapping with our rest-frame *Chandra* band at $z \sim 0$. Considering that the $z \sim 2$ *ROSAT* sources of Yuan et al. (1998a) have values of Γ_X similar to those observed here with *Chandra* at $z \sim 0$, and noting that the source rest-frame energies are approximately the same in these two observed spectra regions, this implies that the soft X-ray spectra of RQQs may be more complex than a simple power-law. In particular, the Yuan et al. (1998a) sources may exhibit a soft excess at $\lesssim 0.3$ keV, causing steeper hardness ratios. Soft excesses have been seen in good-quality spectra of other low- z RQQs (e.g., Gierliński & Done 2004), but the origin of this component is still unclear. If such additional complexity exists, it may be the cause of the steeper values of Γ_X seen in the low- z Yuan et al. (1998a) *ROSAT* sources, and thus the strong anti-correlation between Γ_X and z , and consequently α_{ox} and z , seen by Bechtold et al. (2003).

Although, there is no significant evidence for a Γ_X-z relationship, there is marginally significant evidence (2σ) that Γ_X flattens as z increases. While this may be caused by evolution in Γ_X , it may also represent a systematic flattening of the X-ray continuum at harder energies or the result of a Compton reflection component redshifting into the observed 0.3–7 keV band at higher z . Similarly, a soft excess redshifting out of the observed band may also contribute.

An observed anti-correlation between Γ_X and α_{UV} may result from not fitting an intrinsic absorber to

most of the X-ray spectra. The sources with redder α_{UV} may have higher N_H , which would result in a lower value of Γ_X inferred from the power-law spectral fit. To test this, we estimated the increase in N_H between $\alpha_{UV} \sim 0.1$ and $\alpha_{UV} \sim 1.2$ needed to produce the observed decrease in Γ_X . We used *Sherpa*'s FAKFIT command to simulate spectra assuming a value of $\Gamma_X = 2.2$ and negligible intrinsic neutral absorption, $N_H = 10^{20} \text{ cm}^{-2}$. A value of $\Gamma_X \sim 2.2$ is typical for the bluer sources, $\alpha_{UV} \sim 0.1$. Based on the simulations, N_H must increase to $\sim 10^{21} \text{ cm}^{-2}$ at $\alpha_{UV} \sim 1.2$ to produce an observed decrease of Γ_X from $\Gamma_X \sim 2.2$ to $\Gamma_X \sim 1.8$. We fit an absorbed power-law for the ten reddest sources with > 50 counts, and found that these sources typically had 3σ upper limits of $N_H \lesssim 5 \times 10^{21} \text{ cm}^{-2}$. Values of $N_H \sim 10^{21} \text{ cm}^{-2}$ are well within the limits on N_H at $\alpha_{UV} \sim 1.2$, and therefore we cannot rule out the observed Γ_X - α_{UV} anti-correlation as resulting from unidentified intrinsic absorption.

6.3. Expectation of Accretion Models

Sobolewska et al. (2004a) and Sobolewska et al. (2004b) explored the general parameter space available for accreting compact sources, and quasars in particular, in respect to geometry of the disk and X-ray emitting region. They show that α_{ox} is most sensitive to (1) the amount of energy dissipated in the corona or (2) the size of the inner flow or a structure and outflow velocity of the coronal flares. Sobolewska et al. (2004b) suggest that the α_{ox} - L_{UV} anti-correlation can be explained by differences in the structure of the X-ray emitting region. They point out that in the framework of the truncated disk and hot inner flow geometry, L_{UV} increases when the disk extends further towards the last stable orbit, while Γ_X steepens, reducing the 2 keV emission. In the patchy corona geometry, the α_{ox} - L_{UV} relationship can be explained by changes in the fraction of gravitational energy dissipated in the corona, where a lower fraction results in a weaker and softer (higher Γ_X) X-ray continuum.

The redshift dependence may similarly be explained as resulting from evolution in the accretion geometry. This would imply that for a given L_{UV} , the high redshift sources have larger radii of the inner hot flow sphere or they generate more flares with higher outflow velocities. Both of these explanations imply that Γ_X is also correlated with UV luminosity and anti-correlated with redshift, where Γ_X steepens with increasing L_{UV} and flattens with increasing z . We find no statistically significant evidence for a correlation between Γ_X and L_{UV} , and only marginally significant evidence for an anti-correlation between Γ_X and z . However, it should be noted that there is considerable uncertainty in the regression coefficients, and their joint confidence region is large. While values of zero for the regression coefficients cannot be ruled out, it is interesting to note that the trends of Γ_X with L_{UV} and z implied by the regression are consistent with the model predictions. So long as the accretion disk models do not predict too strong of a relationship between Γ_X and L_{UV} , they may still be consistent with our results.

A dual dependency of α_{ox} on both L_{UV} and z must relate, in current scenarios, to variations in M_{BH} , \dot{m} , and chemical abundances, and their effects on the accretion disk and corona. Unfortunately, the models do not yet predict a specific relationship between α_{ox} and the model parameters, and thus quantitative comparison of our results with the models is difficult; this will be the subject of future research. In addition, the discussion in this section has been model-dependent, and hopefully magneto-hydrodynamic simulations will provide further insight (e.g., De Villiers et al. 2003; Krolik et al. 2005).

6.4. Improving the α_{ox} Analysis

The main source of statistical uncertainty in γ_l and γ_t is the strong degree of correlation between l_{UV} and $t(z)$. For ordinary least-squares regression, the standard errors in the regression coefficients are inflated upwards by a factor of $1/\sqrt{1-r^2}$, where r is the correlation between l_{UV} and $t(z)$ (Fox 1997). For our sample, $r = -0.878$, and therefore the standard errors on the regression coefficients are a factor of ≈ 2 higher than if l_{UV} and $t(z)$ were uncorrelated. Because the anti-correlation between l_{UV} and $t(z)$ is so strong, even a small reduction in this correlation can give a large reduction in the standard errors of γ_l and γ_t . For example, selecting a sample to have $r = -0.7$ will result in a reduction in the standard deviations of γ by about 30%. Future α_{ox} studies should try to select samples that minimize r , as has been done by S06. This, along with the larger sample size and range in luminosity probed by S06, is likely the reason why their confidence regions are smaller (cf., Fig. 9).

Using the fact that the coefficient uncertainties are proportional to $1/\sqrt{1-r^2}$, we investigated whether targeting more faint $z \sim 4$ RQQs with *Chandra* will significantly reduce the standard errors in the regression coefficients. Unfortunately, targeting a reasonable number of additional faint $z \sim 4$ RQQs will not significantly improve the estimates of γ_l and γ_t . Targeting 10 additional RQQs uniformly distribution between $45.5 < \log \nu L_\nu(2500\text{\AA}) < 46.5$ and $3.7 < z < 5$ will only result in a reduction in the standard errors of $\sim 8\%$. Including 30 additional faint, high- z RQQs reduces the standard errors by $\sim 18\%$, but about half of this reduction is the result of the increased sample size.

7. SUMMARY

- There is a significant relationship between α_{ox} , L_{UV} , and $t(z)$, and we did not find any evidence that α_{ox} depends on the UV spectral slope. If we remove the 10 suspected BALs ($z < 1.5$ non-detections), the two best α_{ox} regressions are

$$\begin{aligned} \bar{\alpha}_{\text{ox}} &= (-9.273 \pm 1.241) + (0.233 \pm 0.026)l_{UV} + (2.870 \pm 0.750) \times 10^{-2}t(z), \quad \sigma = 0.125 \\ \bar{\alpha}_{\text{ox}} &= (40.97 \pm 27.34) - (1.949 \pm 1.187)l_{UV} + (2.370 \pm 1.288) \times 10^{-2}l_{UV}^2 + \\ &\quad (2.263 \pm 0.813) \times 10^{-2}t(z), \quad \sigma = 0.124 \end{aligned} \tag{23}$$

Here, the notation $\bar{\alpha}_{\text{ox}}$ denotes the average α_{ox} at a given l_{UV} and $t(z)$, and the intrinsic scatter in α_{ox} at a given l_{UV} and $t(z)$ has a dispersion of $\sigma \approx 0.125$ about $\bar{\alpha}_{\text{ox}}$. Although the l_{UV}^2 term is not ‘statistically significant’ in the classical sense, an analysis based on the Kullback-Leibler information found that this model is best supported by the evidence in our data. The KLI analysis found that both models are preferred over a purely quadratic dependence of α_{ox} on l_{UV} , and over models that parameterized the redshift dependence as linear in z or $\log(1+z)$.

- We used Monte Carlo simulations to show that the $\alpha_{\text{ox}}-z$ relationship is not a spurious result caused by variability and measurement error. Based on the simulations, we calculate the χ^2_2 of our regression coefficients for model \mathcal{M}_t and find that the probability of observing a χ^2_2 this high or higher is $\lesssim 3 \times 10^{-3}$, under the assumption of no evolution in α_{ox} .
- We used Monte Carlo simulations to show that interpretation of Kendall’s generalized partial τ is problematic. In particular, Kendall’s partial τ for the $\alpha_{\text{ox}}-z$ correlation is not necessarily expected to be zero when α_{ox} is unrelated to z , given L_{UV} . Moreover, Kendall’s partial τ is not necessarily expected to be non-zero when α_{ox} is correlated with z , given L_{UV} . This can have a significant effect

on the power of Kendall’s partial τ , and therefore care must be taken when using τ to investigate whether α_{ox} evolves or not. Based on our simulations, we are not able to decide for either evolution or no evolution in α_{ox} using τ .

- The $\alpha_{\text{ox}}-z$ correlation cannot be explained as a result of a systematic steepening of the X-ray continuum at higher energies, as this is inconsistent with the regression of Γ_X on z . Furthermore, the $\alpha_{\text{ox}}-z$ relationship is not the result of soft X-ray neutral absorption shifting out of the observed band. The observed factor of ~ 8 drop in L_X from $z = 4$ to $z = 0$ is higher than the factor of ~ 2 drop in L_X that would result for an unidentified intrinsic neutral absorber with $N_H \sim 10^{21} \text{ cm}^{-2}$. Higher values of N_H are inconsistent with the Γ_X-z results.
- We do not find any evidence for a dependence of Γ_X on UV luminosity, and only marginally significant evidence (2σ) for a dependence of Γ_X on redshift. The Γ_X-z relationship may be caused by a systematic flattening of the X-ray continuum at higher energies, by redshifting of a Compton reflection component into the observed 0.3–7 keV band, and/or by redshifting of a soft excess out of the observable band.
- We find evidence for an anti-correlation (3.5σ) between Γ_X and the UV spectral slope, where the X-ray continuum hardens as the UV continuum softens. This may be the result of unidentified intrinsic absorption, with the UV redder sources having higher intrinsic N_H , thus causing a flatter inferred X-ray continuum.

This research was supported by Chandra Observatory Guest Observer award GO4-5112X, and in part by NASA contract NAS8-39073 (AS, TLA). We are grateful to Martin Elvis for many helpful comments and discussions on this work, Marianne Vestergaard for providing the UV Fe emission template used in this study, and to the anonymous referee for a careful reading and comments that contributed to the significant improvement of this paper.

This research has made use of the NASA/IPAC Extragalactic Database (NED) which is operated by the Jet Propulsion Laboratory, California Institute of Technology, under contract with the National Aeronautics and Space Administration.

Funding for the SDSS and SDSS-II has been provided by the Alfred P. Sloan Foundation, the Participating Institutions, the National Science Foundation, the U.S. Department of Energy, the National Aeronautics and Space Administration, the Japanese Monbukagakusho, the Max Planck Society, and the Higher Education Funding Council for England. The SDSS Web Site is <http://www.sdss.org/>.

The SDSS is managed by the Astrophysical Research Consortium for the Participating Institutions. The Participating Institutions are the American Museum of Natural History, Astrophysical Institute Potsdam, University of Basel, Cambridge University, Case Western Reserve University, University of Chicago, Drexel University, Fermilab, the Institute for Advanced Study, the Japan Participation Group, Johns Hopkins University, the Joint Institute for Nuclear Astrophysics, the Kavli Institute for Particle Astrophysics and Cosmology, the Korean Scientist Group, the Chinese Academy of Sciences (LAMOST), Los Alamos National Laboratory, the Max-Planck-Institute for Astronomy (MPIA), the Max-Planck-Institute for Astrophysics (MPA), New Mexico State University, Ohio State University, University of Pittsburgh, University of Portsmouth, Princeton University, the United States Naval Observatory, and the University of Washington.

A. THE KULLBACK-LEIBLER INFORMATION

The Kullback-Leibler Information (KLI, Kullback & Leibler 1951) is a common method for comparing models and their representation of data. The KLI may be thought of as representing the information lost when a parametric model is used to approximate the true distribution that gave rise to the (Anderson et al. 2000). This approach is appealing because it attempts to find the model that is ‘closest’ to the true distribution. This approach differs from the classical method of statistical hypothesis testing, in that the KLI looks for the model that best describes the data, without assuming that the true model is among the set of models considered. Furthermore, the KLI allows for the comparison of both nested and nonnested models. This is important, because the parametric models considered in Equations (3)–(7) are idealizations that are unlikely to be completely true, and do not form a set of nested parametric forms. However, among these idealizations, we can attempt to find the model that best describes the observed data, while fully admitting that such a model is unlikely to be true exactly. In contrast, the classical approach assumes that some null hypothesis is correct, and then tests whether the model parameters are compatible with this null hypothesis at some set significance level. The significance level is usually set such that, if the null hypothesis is true, then one would incorrectly reject it with low probability. In other words, the classical approach assumes that a ‘null’ model is correct, and then looks for overwhelming evidence to the contrary. However, a comparison of models based on the KLI does not make any *a priori* assumptions about which model is correct, but rather assesses which (flawed) model best describes the observed data; i.e., is ‘closest’ to the true probability density that generated the data. In this sense, the KLI evaluates the evidence *for* the models considered, whereas the classical approach only evaluates the evidence *against* some assumed null model. In addition, comparing models based on the KLI has the advantage that all models may be compared simultaneously, whereas the classical approach can only compare two models at a time.

Problems with the classical approach to statistical hypothesis testing and model selection have been known for some time, and many authors have proposed using the KLI as an alternative (e.g., Akaike 1974). There is a large literature on these issues; see Anderson et al. (2000) and references therein for a more thorough discussion of the problems with classical hypothesis testing and the advantages of the information-theoretic approach.

The KLI measures the discrepancy between the model distribution for the data, $p(y|\theta)$, parameterized by θ , and the true distribution of the data $f(y)$; note that $p(y|\theta)$ is the likelihood function for y . The KLI may be thought of as the relative entropy of a statistical model, and is given by

$$H(\theta) = \int \log \left(\frac{f(y)}{p(y|\theta)} \right) f(y) dy. \tag{A1}$$

The difference in KLI between two statistical models, $p_j(y|\theta_j)$ and $p_k(y|\theta_k)$, is then

$$H(\theta_j) - H(\theta_k) = \int [\log p_k(y|\theta_k) - \log p_j(y|\theta_j)] f(y) dy. \tag{A2}$$

As is apparent from Equation (A2), the difference in KLI between two statistical models is the expectation of the difference in their log-likelihoods, multiplied by -1. The Kullback-Leibler information describes the information lost when a statistical model, $p(y|\theta)$, is used to approximate the true distribution, $f(y)$.

For this work $y = \alpha_{\text{ox}}$, and the true sampling distribution of α_{ox} is denoted as $f(\alpha_{\text{ox}}|l_{UV}, z)$. The distribution is made conditional on (l_{UV}, z) because we are interested in how α_{ox} is distributed at a given l_{UV} and z .

In order to choose the model that minimizes the KLI, it is necessary to find the values of the model parameters, θ , that minimize Equation (A1). Unfortunately, this requires knowledge of the unknown sampling density, $f(\alpha_{\text{ox}}|l_{UV}, z)$. However, the maximum likelihood estimate of θ , $\hat{\theta}$, provides a good estimate of the θ that minimizes the KLI, and in fact converges to it as the sample size becomes large (e.g., Shibata 1997). Furthermore, for non-censored Gaussian data, $\hat{\theta}$ corresponds to the θ that minimizes the squared error between the data and the model predictions, and thus finding the model that minimizes the KLI is asymptotically equivalent to finding the model that minimizes the expected squared error. In this work the amount of censoring is small, and the censored data only contribute to the log-likelihood at the $\approx 5\%$ level. Because the residuals from the α_{ox} regressions are approximately Gaussian, and because the amount of censoring is small, we expect our statistical models to behave similarly to the usual uncensored case for Gaussian data. Therefore, finding the parameterization that minimizes the KLI has the straight-forward interpretation of finding the parameterization that approximately minimizes the expected squared error.

Because the difference in KLI between two models is the expected difference in their log-likelihoods, one can estimate $H(\hat{\theta}_j) - H(\hat{\theta}_k)$ for a single data point using the sample mean of the difference in log-likelihoods, evaluated at the maximum likelihood estimates of θ . However, this produces a biased estimate of $H(\theta_j) - H(\theta_k)$, as we use the same data to fit the model as to estimate its KLI. Akaike (1974) showed that this bias is on the order of the number of free parameters in the statistical model. This led him to define the Akaike Information Criterion (AIC):

$$AIC = -2 \log p(y|\hat{\theta}) + 2d. \tag{A3}$$

Here, $\log p(y|\hat{\theta})$ is the log-likelihood of the data evaluated at the maximum-likelihood estimate of θ , and d is the number of free parameters in the model. The differences in AIC between models may then be used as estimates of the differences in KLI between the models. The model with the best estimated KLI is the model that minimizes the AIC .

B. Kendall's Partial τ

To further assess the behavior of Kendall's partial τ we performed additional simulations, varying the degree of correlation between L_{UV} and z . We drew 165 values of l_{UV} and $\log z$ from a multivariate normal density for 1000 simulations, with correlations between l_{UV} and $\log z$ of $\rho = 0.0, 0.3, 0.6$, and 0.9 . The remainder of the simulations were performed in an identical manner to those described in § 3.5 and § 3.6, with the exception that we did not include the effects of variability and measurement error. For each of these cases, we calculated the average values of $\tau_{xz,l}$ and $\tau_{\alpha z,l}$ under both the null and alternative hypotheses. From the notation of § 3.6, $\tau_{xz,l}$ denotes the value of Kendall's partial τ between L_X and z , controlling for L_{UV} , and $\tau_{\alpha z,l}$ denotes the value of Kendall's partial τ between α_{ox} and z , controlling for L_{UV} .

In addition, we also calculate the power of the test when using either $\tau_{xz,l}$ and $\tau_{\alpha z,l}$ under both hypotheses; the power of a statistical test is the probability of choosing for the alternative hypothesis. We have chosen a significance level of 0.05, meaning that we reject the null hypothesis, H_0 , when $|\tau - E(\tau|H_0)|/\sigma_\tau > 1.96$, where σ_τ is the standard deviation in τ . Here, the notation $E(x|H)$ denotes the conditional expectation value of x , given hypothesis H . Using this significance level, we would expect to incorrectly reject the null hypothesis $\approx 5\%$ of the time. To illustrate the effect of incorrectly assuming that $E(\tau|H_0) = 0$, we calculate the power assuming $E(\tau|H_0) = 0$. Therefore, the null hypothesis is rejected when the observed value of τ falls within the region, $|\tau| > 1.96\sigma_\tau$.

The results of our simulations are shown in Table 5. As can be seen, incorrectly assuming $E(\tau|H_0) = 0$

has a significant effect on the conclusions drawn from Kendall’s generalized partial τ . This is particularly notable when the correlation between the two ‘independent’ variables is high, in this case between L_{UV} and z . For high correlations between L_{UV} and z , one incorrectly rejects the null hypothesis with probability $p \approx 0.988$ when using $\tau_{xz,l}$, and $p \approx 0.845$ when using $\tau_{\alpha z,l}$. Furthermore, when L_{UV} and z are highly correlated and one is using $\tau_{\alpha z,l}$, one rarely ($p \approx 0.061$) rejects the null hypothesis if the alternative hypothesis is true. However, one does reject the null hypothesis when the alternative is true with near certainty when using $\tau_{xz,l}$. These problems are ameliorated when the degree of correlation between the independent variables is reduced; however, even when $\rho = 0.3$ one still incorrectly rejects the null hypothesis with probability a factor of ~ 2 – 4 times higher than the expected 5%.

We also performed our simulations experimenting with different sample sizes. We did not notice any dependence of $E(\tau|H_0)$ on the sample size. This results in the seemingly paradoxical behavior that, as the sample size increases, the null hypothesis is rejected with increasing probability even if it is true, if one assumes $E(\tau|H_0) = 0$. While the expected value of τ under the null hypothesis does not appear to depend on sample size, the variance in τ , σ_τ^2 , does, decreasing as the sample size increases. Thus, as the sample size increases, σ_τ decreases, and the observed values of τ become more concentrated around $E(\tau|H_0)$. As a result, if one incorrectly assumes $E(\tau|H_0) = 0$, it becomes more likely that τ falls inside of the region where $|\tau| > 1.96\sigma_\tau$, and thus one is more likely to incorrectly reject the null hypothesis as the sample size increases.

Similar results using Monte Carlo Simulations were found by Steffen et al. (2006). S06 concluded that their results implied that spurious but false correlations between L_X and z result when there is a high degree of correlation between L_{UV} and z . However, the results do not imply that spurious but false correlation arise when there is a high degree of correlation between L_{UV} and z , but rather the simulations show that the expected value of τ under the null hypothesis varies as the degree of correlation between L_{UV} and z varies. This may then result in apparently significant correlations because one is incorrectly assuming $E(\tau|H_0) = 0$. This incorrect assumption can also result in apparently insignificant correlations, even if such correlations are significant. Our simulations clearly show this, since they were constructed to ensure that under the null hypothesis α_{ox} is independent of z , given L_{UV} ,, *independent* of the distribution of L_{UV} and z .

Akritis & Siebert (1996) also performed simulations to assess the behavior of Kendall’s partial τ . They investigated the power of the test and found that the test becomes more powerful as the departure from the null hypothesis increases. They also found that when the null hypothesis is true, and when the two independent variable are statistically independent, the probability of rejecting H_0 is equal to the chosen significance level. Similar to us, they also use a significance level of 0.05 (1.96σ). However, when investigating the probability of incorrectly rejecting the null hypothesis, they only used simulations where the two independent variables (L_{UV} and z in this work) are statistically independent. We have confirmed this result here, but have also expanded upon it, showing that the null hypothesis can be incorrectly rejected with high probability when the two independent variables have a moderate to high correlation. Furthermore, Akritis & Siebert (1996) concluded that the Kendall’s partial τ test can become more powerful when the alternative hypothesis is far from the null hypothesis, rejecting the null hypothesis with high probability. However, we have shown here that this is not always true, and that the power of the test depends on the degree of correlation between the two independent variables. Indeed, when L_{UV} and z are highly correlated, and when one is investigating the partial correlation between α_{ox} and z , one almost always incorrectly claims that the data are consistent with a null hypothesis of no evolution in α_{ox} .

It should be noted that these results only apply to Kendall’s *partial* τ , and not to the usual Kendall’s τ . Both Kendall’s τ and the partial linear correlation have values of zero under the null hypothesis of statistical independence between the variables of interest (Nelson & Yang 1988).

Our simulations show that the expected value of Kendall's partial τ under the null hypothesis depends on the distributional properties of the sample, and that this can significantly effect the power of the test. Unfortunately, we know of no way in which to analytically calculate the expected value of τ under the null hypothesis, and it must likely be calculated using simulation. However, one must likely employ parametric methods in order to simulate data, and this undermines the nonparametric nature of Kendall's partial τ . We also note that these results are not meant to be a complete dismissal of the use of Kendall's generalized partial τ , but rather to point out the problems that can arise when using Kendall's partial τ . If one does not know $E(\tau|H_0)$, then one is not able to calibrate the partial τ statistic against a physically meaningful null hypothesis, therefore making statistical hypothesis testing based on it suspect.

REFERENCES

- Aitken, M. 1981, *Technometrics*, 23, 161
- Akaike, H. 1974, *IEEE Transactions on Automatic Control*, 19, 716
- Akritas, M. G., & Bershad, M. A. 1996, *ApJ*, 470, 706
- Akritas, M. G., & Siebert, J. 1996, *MNRAS*, 278, 919
- Anderson, D. R., Burnham, K. P., Thompson, W. L. 2000, *J. Wildl. Manage.*
- Anderson, S. F., et al. 2001, *AJ*, 122, 503
- Avni, Y., & Tananbaum, H. 1982, *ApJ*, 262, L17
- Avni, Y., & Tananbaum, H. 1986, *ApJ*, 305, 83 (AT86)
- Bechtold, J., et al. 2003, *ApJ*, 588, 119
- Bisnovatyi-Kogan, G. S., & Blinnikov, S. I. 1977, *A&A*, 59, 111
- Brockopp, C., Starling, R. L. C., Schady, P., Mason, K. O., Romero-Colmenero, E., & Puchnarewicz, E. M. 2006, *MNRAS*, 366, 953
- Budavári, T., et al. 2005, *ApJ*, 619, L31
- Cardelli, J. A., Clayton, G. C., & Mathis, J. S. 1989, *ApJ*, 345, 245
- Cash, W. 1979, *ApJ*, 228, 939
- Constantin, A., Shields, J. C., Hamann, F., Foltz, C. B., & Chaffee, F. H. 2002, *ApJ*, 565, 50
- Dai, X., Chartas, G., Eracleous, M., & Garmire, G. P. 2004, *ApJ*, 605, 45
- Dempster, A., Laird, N., & Rubin, D. 1977, *J. R. Statist. Soc. B.*, 39, 1
- De Villiers, J.-P., Hawley, J. F., & Krolik, J. H. 2003, *ApJ*, 599, 1238
- Dickey, J. M., & Lockman, F. J. 1990, *ARA&A*, 28, 215
- Efron, B. 1979, *Ann. Statist.*, 7, 1

- Efron, B. 1984, *J. Amer. Stat. Assoc.*
- Feigelson, E. D., & Nelson, P. I. 1985, *ApJ*, 293, 192
- Fox, J. 1997, *Applied Regression Analysis, Linear Models, and Related Methods* (Thousand Oaks:Sage Publications, Inc.)
- Freeman, P. E., Graziani, C., Lamb, D. Q., Lored, T. J., Fenimore, E. E., Murakami, T., & Yoshida, A. 1999, *ApJ*, 524, 753
- Freeman, P. E., Doe, S., & Siemiginowska, A. 2001, *SPIE Proceedings*, 4477, 76
- Galeev, A. A., Rosner, R., & Vaiana, G. S. 1979, *ApJ*, 229, 318
- Gallagher, S. C., Brandt, W. N., Chartas, G., & Garmire, G. P. 2002, *ApJ*, 567, 37
- Gallagher, S. C., Richards, G. T., Hall, P. B., Brandt, W. N., Schneider, D. P., & Vanden Berk, D. E. 2005, *AJ*, 129, 567
- Gallagher, S. C., Brandt, W. N., Chartas, G., Priddey, R., Garmire, G. P., & Sambruna, R. M. 2006, *ApJ*, 644, 709
- Gelman, A., Carlin, J. B., Stern, H. S., & Rubin, D. B. 2004, *Bayesian Data Analysis* (2nd ed.; Boca Raton:Chapman & Hall/CRC)
- Gierliński, M., & Done, C. 2004, *MNRAS*, 349, L7
- Green, P. J., Aldcroft, T. L., Mathur, S., Wilkes, B. J., & Elvis, M. 2001, *ApJ*, 558, 109
- Grupe, D., Thomas, H.-C., & Beuermann, K. 2001, *A&A*, 367, 470
- Grupe, D., Mathur, S., Wilkes, B., & Osmer, P. 2006, *AJ*, 131, 55
- Hastie, T., Tibshirani, R., & Friedman, J. 2001, *The Elements of Statistical Learning* (New York:Springer-Verlag)
- Isobe, T., Feigelson, E. D., & Nelson, P. I. 1986, *ApJ*, 306, 490
- Ivezić, Z., et al. 2004, *ASP Conf. Ser.* 311: AGN Physics with the Sloan Digital Sky Survey, 311, 347
- Janiuk, A., & Czerny, B. 2000, *New Astronomy*, 5, 7
- Kennefick, J. D., de Carvalho, R. R., Djorgovski, S. G., Wilber, M. M., Dickson, E. S., Weir, N., Fayyad, U., & Roden, J. 1995, *AJ*, 110, 78
- Krolik, J. H., Hawley, J. F., & Hirose, S. 2005, *ApJ*, 622, 1008
- Kullback, S., & Leibler, R. A. 1951, *Ann. Math. Statist.*, 22, 76
- La Franca, F., et al. 2005, *ApJ*, 635, 864
- Liang, E. P. T., & Price, R. H. 1977, *ApJ*, 218, 247
- Lu, Y., & Yu, Q. 1999, *ApJ*, 526, L5
- Malzac, J., Beloborodov, A. M., & Poutanen, J. 2001, *MNRAS*, 326, 417

- Markowitz, A., Edelson, R., & Vaughan, S. 2003, *ApJ*, 598, 935
- Nayakshin, S. 2000, *ApJ*, 534, 718
- Nelson, P. I., & Yang, S. S., 1988, *Statis.Prob.Lett.*, 6, 147
- Page, K. L., Turner, M. J. L., Reeves, J. N., O'Brien, P. T., & Sembay, S. 2003, *MNRAS*, 338, 1004
- Péroux, C., Storrie-Lombardi, L. J., McMahon, R. G., Irwin, M., & Hook, I. M. 2001, *AJ*, 121, 1799
- Piconcelli, E., Cappi, M., Bassani, L., Di Cocco, G., & Dadina, M. 2003, *A&A*, 412, 689
- Piconcelli, E., Jimenez-Bailón, E., Guainazzi, M., Schartel, N., Rodríguez-Pascual, P. M., & Santos-Lleó, M. 2005, *A&A*, 432, 15
- Poutanen, J., Krolik, J. H., & Ryde, F. 1997, *MNRAS*, 292, L21
- Press, W. H., Teukolsky, S. A., Vetterling, W. T., & Flannery, B. P. 1992, *Numerical Recipes (Second ed.; Cambridge:Cambridge Univ. Press)*, 660
- Proga, D. 2005, *ApJ*, 630, L9
- Protassov, R., van Dyk, D. A., Connors, A., Kashyap, V. L., & Siemiginowska, A. 2002, *ApJ*, 571, 545
- Reeves, J. N., Turner, M. J. L., Ohashi, T., & Kii, T. 1997, *MNRAS*, 292, 468
- Reeves, J. N., & Turner, M. J. L. 2000, *MNRAS*, 316, 234
- Reichard, T. A., et al. 2003, *AJ*, 126, 2594
- Richards, G. T., et al. 2001, *AJ*, 121, 2308
- Richards, G. T., et al. 2002, *AJ*, 123, 2945
- Risaliti, G., & Elvis, M. 2005, *ApJ*, 629, L17
- Schlegel, D. J., Finkbeiner, D. P., & Davis, M. 1998, *ApJ*, 500, 525
- Schmidt, M., & Green, R. F. 1983, *ApJ*, 269, 352
- Schneider, D. P., Schmidt, M., & Gunn, J. E. 1991, *AJ*, 101, 2004
- Schneider, D. P., Schmidt, M., & Gunn, J. E. 1997, *AJ*, 114, 36
- Schneider, D. P., et al. 2005, *AJ*, 130, 367
- Shapiro, S. L., Lightman, A. P., & Eardley, D. M. 1976, *ApJ*, 204, 187
- Shemmer, O., et al. 2006, *ApJ*, 644, 86
- Shemmer, O., Brandt, W. N., Netzer, H., Maiolino, R., & Kaspi, S. 2006, *ApJ*, 646, L29
- Shibata, R. 1997, *Statistica Sinica*, 7, 375
- Silverman, B. 1986, *Density Estimation for Statistics and Data Analysis (London:Chapman and Hall)*
- Silverman, J. D., et al. 2005, *ApJ*, 618, 123

- Sobolewska, M. A., Siemiginowska, A., & Życki, P. T. 2004a, *ApJ*, 608, 80
- Sobolewska, M. A., Siemiginowska, A., & Życki, P. T. 2004b, *ApJ*, 617, 102
- Spergel, D. N., et al. 2003, *ApJS*, 148, 175
- Stapleton, D. C. & Young, D. J. 1984, *Econometrica*, 52, 737
- Steffen, A. T., Strateva, I., Brandt, W. N., Alexander, D. M., Koekemoer, A. M., Lehmer, B. D., Schneider, D. P., & Vignali, C. 2006, *AJ*, 131, 2826 (S06)
- Storrie-Lombardi, L. J., McMahon, R. G., Irwin, M. J., & Hazard, C. 1996, *ApJ*, 468, 121
- Strateva, I. V., Brandt, W. N., Schneider, D. P., Vanden Berk, D. G., & Vignali, C. 2005, *AJ*, 130, 387 (S05)
- Tananbaum, H., et al. 1979, *ApJ*, 234, L9
- Tremaine, S., et al. 2002, *ApJ*, 574, 740
- Uttley, P., McHardy, I. M., & Papadakis, I. E. 2002, *MNRAS*, 332, 231
- Véron-Cetty, M.-P., Joly, M., & Véron, P. 2004, *A&A*, 417, 515
- Vestergaard, M., & Wilkes, B. J. 2001, *ApJS*, 134, 1
- Vignali, C., Comastri, A., Cappi, M., Palumbo, G. G. C., Matsuoka, M., & Kubo, H. 1999, *ApJ*, 516, 582
- Vignali, C., Brandt, W. N., Fan, X., Gunn, J. E., Kaspi, S., Schneider, D. P., & Strauss, M. A. 2001, *AJ*, 122, 2143
- Vignali, C., Brandt, W. N., Schneider, D. P., Garmire, G. P., & Kaspi, S. 2003, *AJ*, 125, 418
- Vignali, C., Brandt, W. N., & Schneider, D. P. 2003, *AJ*, 125, 433
- Vignali, C., et al. 2003, *AJ*, 125, 2876
- Vignali, C., Brandt, W. N., Schneider, D. P., & Kaspi, S. 2005, *AJ*, 129, 2519
- Wang, J.-M., Watarai, K.-Y., & Mineshige, S. 2004, *ApJ*, 607, L107
- Wilkes, B. J., & Elvis, M. 1987, *ApJ*, 323, 243
- Wilkes, B. J., Tananbaum, H., Worrall, D. M., Avni, Y., Oey, M. S., & Flanagan, J. 1994, *ApJS*, 92, 53 (W94)
- Wolf, C., et al. 2004, *A&A*, 421, 913
- Worrall, D. M., Tananbaum, H., Giommi, P., & Zamorani, G. 1987, *ApJ*, 313, 596
- York, D. G., et al. 2000, *AJ*, 120, 1579
- Yuan, W., Brinkmann, W., Siebert, J., & Voges, W. 1998a, *A&A*, 330, 108
- Yuan, W., Siebert, J., & Brinkmann, W. 1998b, *A&A*, 334, 498
- Zamorani, G., et al. 1981, *ApJ*, 245, 357
- Zdziarski, A. A., Lubinski, P., & Smith, D. A. 1999, *MNRAS*, 303, L11

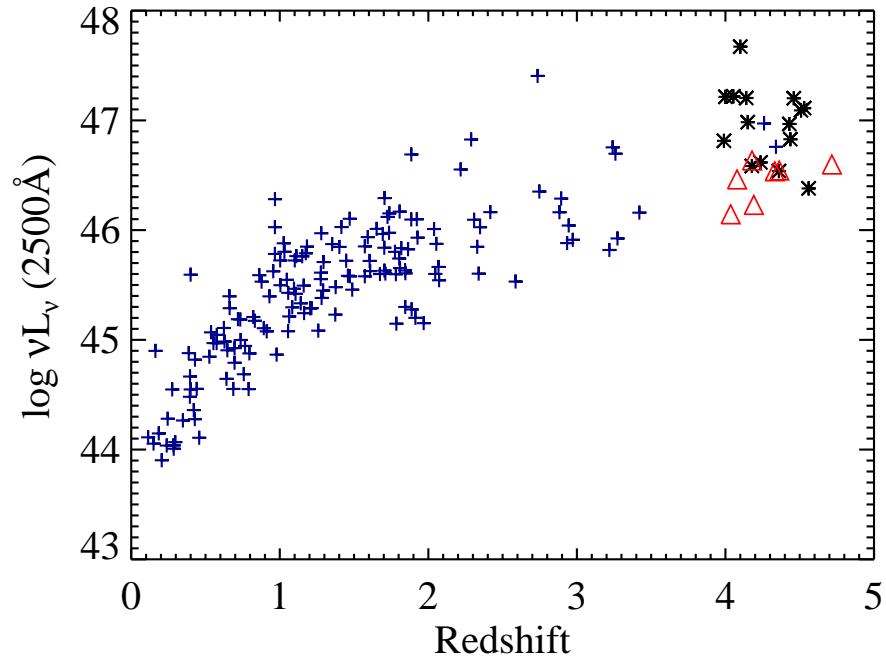


Fig. 1.— The (L_{UV}, z) distribution of our sample. The seven new observations are denoted by red triangles, the SDSS sources are denoted by blue crosses, and the non-SDSS $z \gtrsim 4$ sources are denoted by black asterisks. There appears to be data points for only six RQQs with new *Chandra* observations because sources 0050-0053 and 2357+0053 have almost the same L_{UV} and z , causing their symbols to overlap.

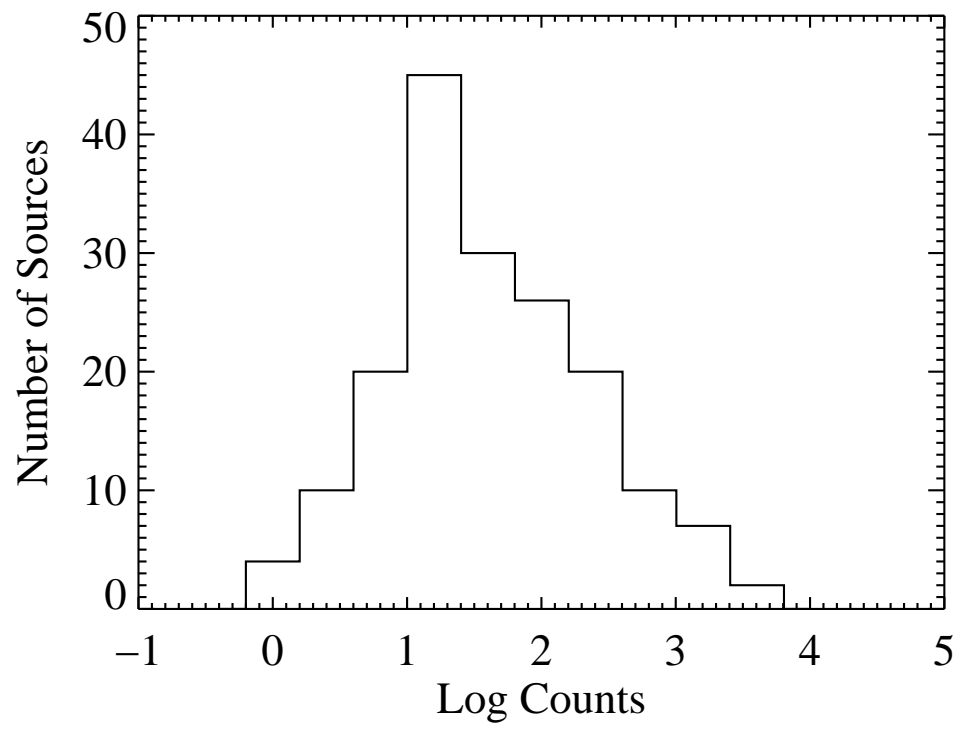


Fig. 2.— The distribution of observed, background-subtracted, 0.3–7.0 keV photon counts for our sample.

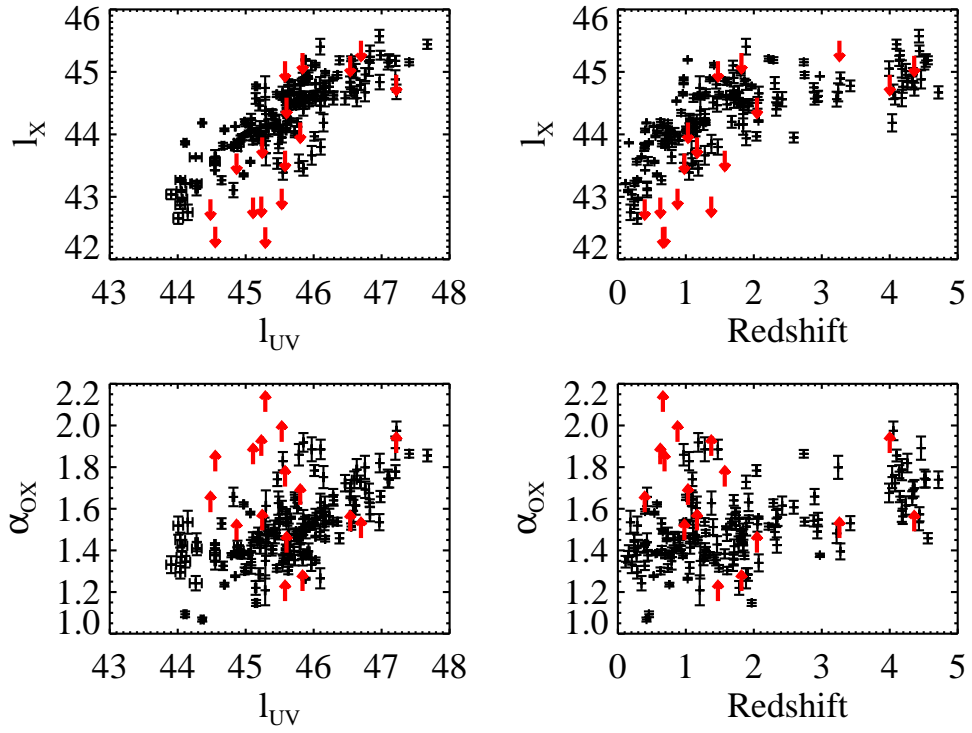


Fig. 3.— The distribution of l_X and α_{ox} as functions of l_{UV} and z . Red arrows denote upper limits for l_X and lower limits of α_{ox} .

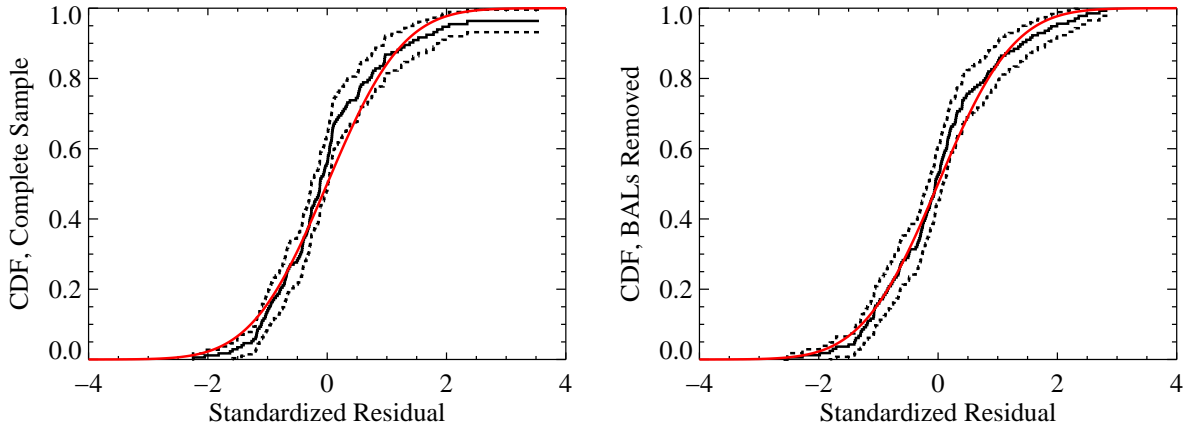


Fig. 4.— Empirical cumulative distribution functions (CDF) of the standardized residuals for the regression of α_{ox} on l_{UV} and $t(z)$ using the complete sample (left), and after removing suspected BALs (all $z < 1.5$ censored data points), right. The red line is the standard normal CDF, and the dashed lines denote the 95% pointwise confidence interval on the empirical CDF. The CDF of the standardized residuals for the full sample shows evidence of diverging from normality, while the CDF of the sample with suspected BALs removed is consistent with the assumption of normality.

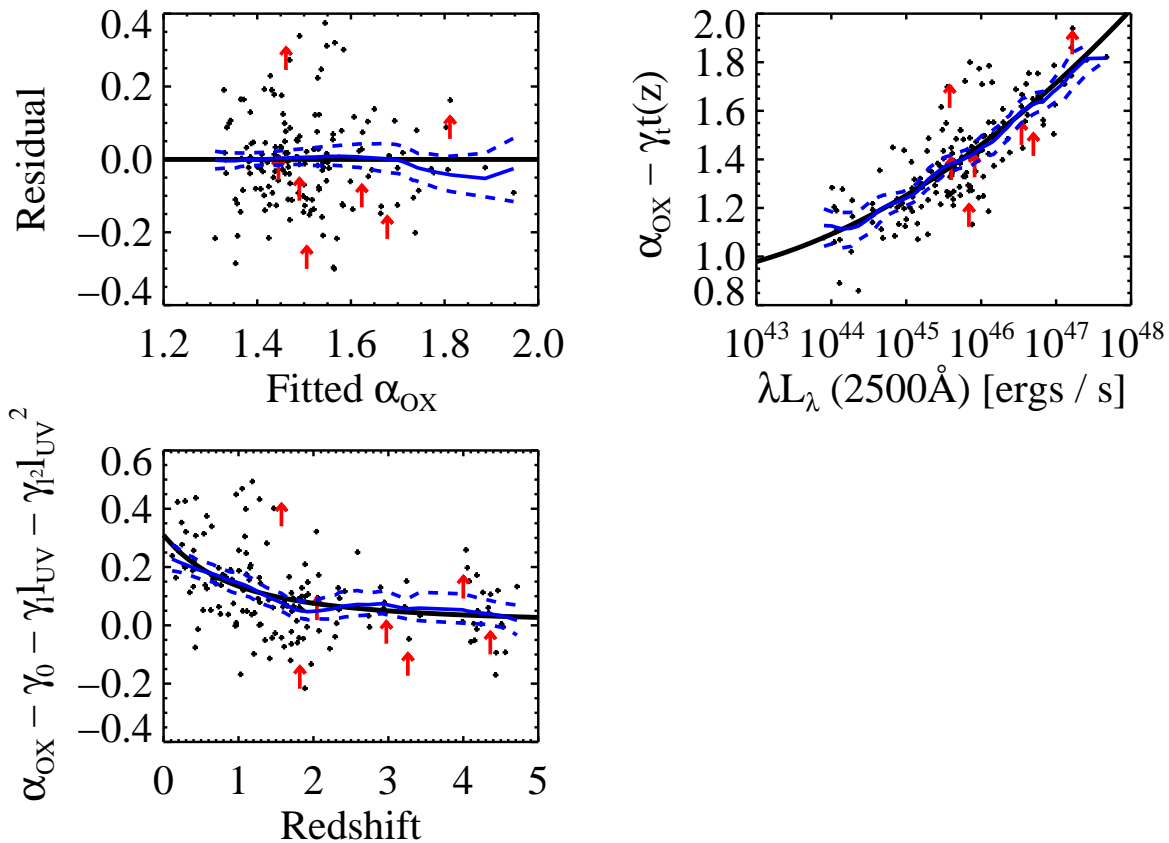


Fig. 5.— The residuals of the α_{ox} regression for model \mathcal{M}_{l+t} , shown as a function of the fitted α_{ox} , and partial residuals shown as functions of L_{UV} and z . The partial residual plots show the dependence of α_{ox} on L_{UV} or z , after accounting for the dependence of α_{ox} on z or L_{UV} . Also shown are kernel-smoother fits to the residuals (solid blue lines), as well as approximate 95% pointwise confidence intervals on the kernel-smoother fits (dashed blue lines).

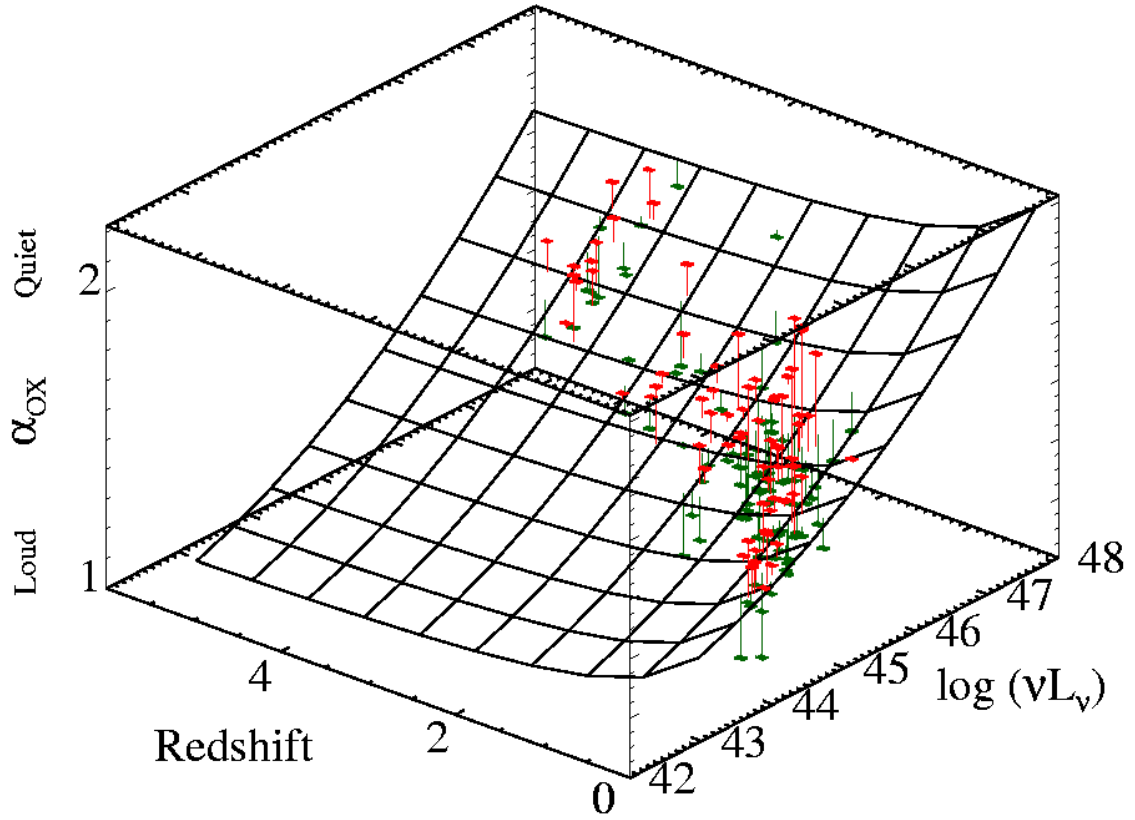


Fig. 6.— The 3-dimensional distribution of α_{ox} , l_{UV} , and z . The surface is the best fit to the data, obtained with model \mathcal{M}_{l+t} . Red denotes data points that fall above the fit, green denotes data points that fall below the fit.

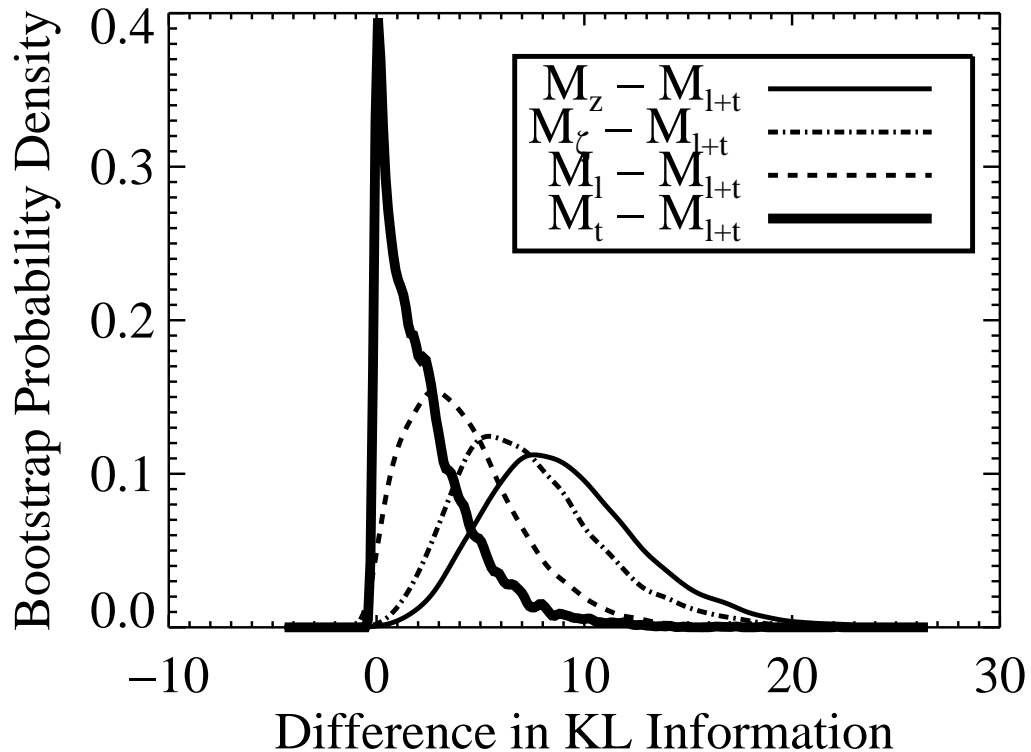


Fig. 7.— Sampling distributions of the difference in Kullback-Leibler information relative to the $t(z)$ parameterization with quadratic l_{UV} term, \mathcal{M}_{l+t} , as determined from bootstrapping. Shown are the estimated distributions of the difference in KLI between \mathcal{M}_z and \mathcal{M}_{l+t} (thin solid line), \mathcal{M}_ζ and \mathcal{M}_{l+t} (dot-dashed line), \mathcal{M}_l and \mathcal{M}_{l+t} (dashed line), and \mathcal{M}_t and \mathcal{M}_{l+t} (thick solid line). As can be seen, the $t(z)$ parameterization with quadratic l_{UV} term is almost always preferred.

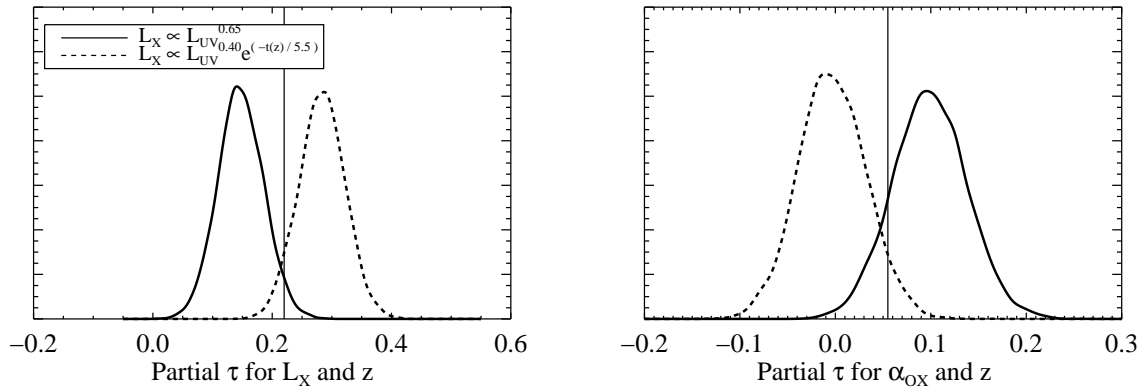


Fig. 8.— Distribution of Kendall’s generalized partial τ for L_X and z (left) and α_{ox} and z (right) under the no-evolution hypothesis (solid line) and the evolution hypothesis (dashed line). The vertical lines show the observed values of τ for our sample. As can be seen, our value of τ is about as consistent with the evolution model as with the no-evolution model. Also, note that $\tau \neq 0$ under the null hypothesis of no evolution (i.e., statistical independence of α_{ox} and z given L_{UV}), and therefore it is incorrect to calculate significance levels with respect to $\tau = 0$.

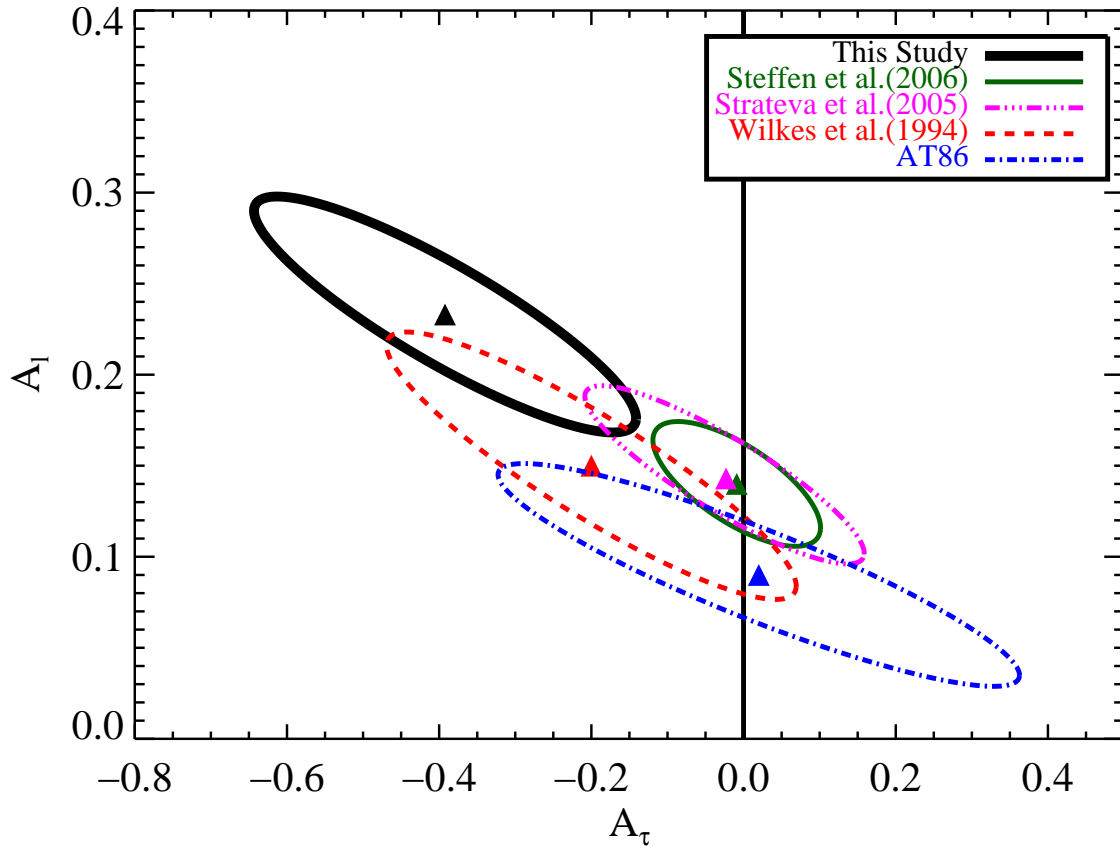


Fig. 9.— Comparison of our values of A_l and A_τ with AT86 (blue, dashed-dotted contour), W94 (red, dashed contour), S05 (magenta, dash-dot-dot-dot contour), and S06 (green, solid thin contour). The estimates of (A_l, A_τ) are denoted by triangles and the ellipses are approximate 95% (2σ) confidence regions.

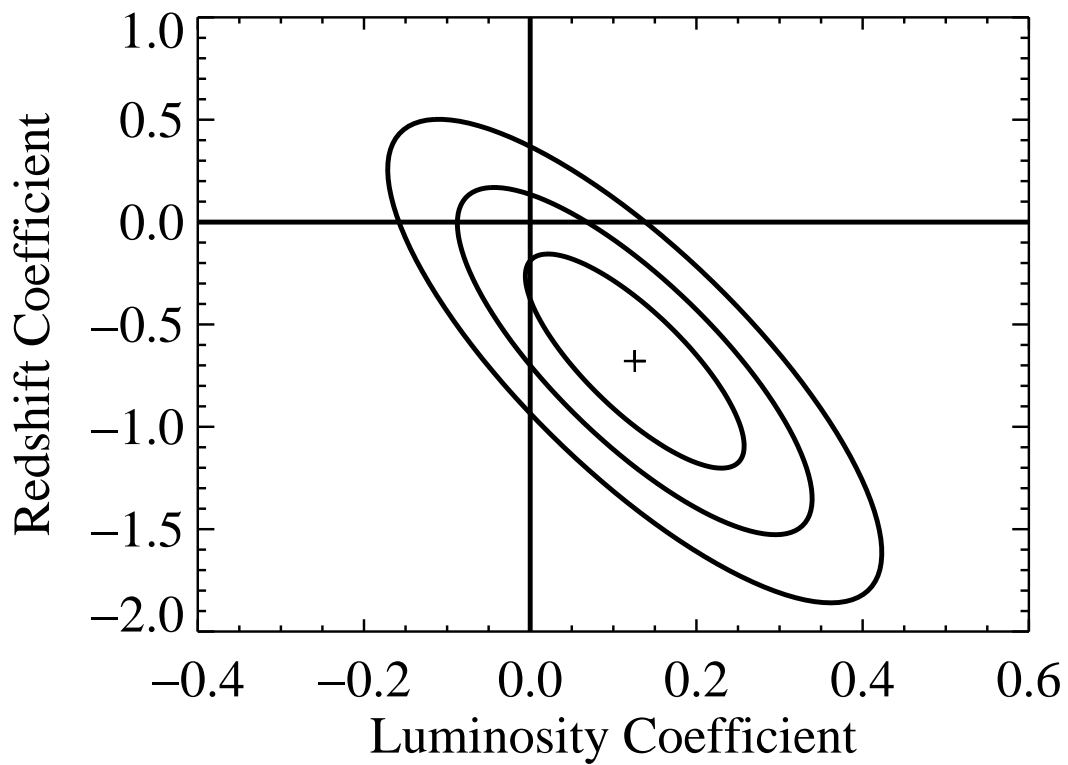


Fig. 10.— Confidence regions for the l_{UV} and $\log(1+z)$ coefficients in the regression of Γ_X on l_{UV} and $\log(1+z)$. The cross denotes the best-fit value, and the contours are the 68%, 95%, and 99.7% joint confidence regions.

Table 1. List of New Observations

Source	RA J2000	DEC J2000	z	r^a	OBSID	Counts ^b	f_X^c 10^{-15} ergs cm ⁻² s ⁻¹	Exp. Time ksec	Spec. Ref. ^d	Phot. Ref. ^e
SDSS 0050-0053	00 50 06.3	-00 53 19.0	4.331	20.13	4825	26.3	6.91 ± 1.38	13.0	1	1
Q 0910+564	09 14 39.3	+56 13 21.0	4.035	20.87	4821	13.4	1.79 ± 0.57	23.0	2	2
SDSS 1321+0038	13 21 10.8	+00 38 22.0	4.716	21.30	4824	19.8	3.88 ± 0.87	17.8	1	1
SDSS 1413+0000	14 13 15.3	+00 00 32.0	4.078	19.75	4823	23.0	4.33 ± 1.02	12.5	1	1
SDSS 1444-0123	14 44 28.7	-01 23 44.0	4.179	19.64	4826	12.1	4.12 ± 1.26	10.0	1	1
PC 1450+3404	14 53 00.6	+33 52 06.0	4.191	20.81	4822	20.2	6.20 ± 1.36	14.8	3	4
SDSS 2357+0043	23 57 18.3	+00 43 50.0	4.362	19.92	4827	19.7	5.20 ± 1.23	12.7	1	1

^a r -band apparent magnitude.

^bNumber of observed background-subtracted source counts in the range 0.3–7.0 keV.

^cUnabsorbed 2–10 keV flux, assuming a power law with $\Gamma_X = 1.9$.

^dReference for the observed frame optical spectrum.

^eReference for the r -band magnitude.

References. — (1) SDSS; (2) Schneider et al. (1991); (3) Constantin et al. (2002); (4) Schneider et al. (1997)

Table 2. List of Archival Sources

Source	RA J2000	DEC J2000	z	r^a	OBSID	θ^b	Counts ^c	Exp. Time ksec	f_X^d 10^{-14} ergs cm^{-2} s^{-1}	Spec. Ref. ^e	Phot. Ref. ^f
0002+0049	00 02 30.7	+00 49 59.0	1.352	18.12	4861	0.58	188.0	5.7	10.52 ± 1.07	1	1
0006-0015	00 06 54.1	-00 15 33.4	1.725	18.20	4096	0.58	46.2	4.5	3.35 ± 0.49	1	1
0022+0016	00 22 10.0	+00 16 29.3	0.574	18.06	2252	7.12	343.4	71.2	2.82 ± 0.48	1	1
0027+0026	00 27 52.4	+00 26 15.7	0.205	18.18	4080	4.48	54.4	1.6	11.66 ± 4.47	1	1
0031+0034	00 31 31.4	+00 34 20.2	1.735	18.79	2101	1.20	73.9	6.7	3.10 ± 0.51	1	1
0057+1450	00 57 01.1	+14 50 03.0	0.623	18.81	865	1.15	4.6	4.6	< 0.91	1	1
0059+0003	00 59 22.8	+00 03 01.0	4.178	19.5	2179	0.58	9.0	2.7	1.21 ± 0.38	2	5
0106+0048	01 06 19.2	+00 48 22.0	4.437	19.1	2180	0.60	24.2	3.7	2.04 ± 0.41	2	5
0113+1531	01 13 05.7	+15 31 46.5	0.576	18.30	3219	2.09	1291.8	58.5	12.41 ± 0.53	1	1
0113+1535	01 13 09.1	+15 35 53.6	1.806	18.33	3219	6.29	528.3	58.5	6.20 ± 0.29	1	1
0115+0020	01 15 37.7	+00 20 28.7	1.275	18.72	3204	6.79	406.2	37.6	6.77 ± 0.66	1	1
0133+0400	01 33 40.4	+04 00 59.0	4.150	18.0	3152	0.59	39.4	6.1	2.03 ± 0.33	3	3
0134+3307	01 34 21.5	+33 07 56.6	4.530	18.9	3018	0.60	22.7	5.0	1.38 ± 0.32	3	3
0148+0001	01 48 12.2	+00 01 53.3	1.704	17.67	4098	0.57	42.3	3.7	3.57 ± 0.55	1	1
0148-0002	01 48 21.0	-00 02 25.8	0.930	18.39	4098	5.41	94.7	3.7	7.96 ± 1.53	1	1
0152+0105	01 52 58.7	+01 05 07.4	0.647	19.22	1448	4.13	104.6	7.9	6.86 ± 1.30	1	1
0153+0052	01 53 09.1	+00 52 50.1	1.161	18.81	3580	7.26	58.1	19.9	2.27 ± 0.37	1	1
0156+0053	01 56 50.3	+00 53 08.5	1.652	18.65	4100	0.59	95.2	5.6	4.58 ± 0.49	1	1
0159+0023	01 59 50.2	+00 23 40.8	0.162	15.97	4104	0.58	5708.2	9.7	189.5 ± 8.19	1	1
0201-0919	02 01 18.7	-09 19 35.8	0.660	17.61	3772	7.83	379.2	19.7	11.42 ± 1.17	1	1
0208+0022	02 08 45.5	+00 22 36.1	1.885	17.08	4099	0.58	58.2	3.5	4.69 ± 0.65	1	1
0209+0517	02 09 44.7	+05 17 14.0	4.140	17.8	3153	0.60	30.2	5.8	1.66 ± 0.31	3	3
0232-0731	02 32 17.7	-07 31 19.9	1.163	19.19	3030	10.1	0.0	4.2	< 1.85	1	1
0241-0811	02 41 05.8	-08 11 53.2	0.978	19.87	385	1.69	5.8	2.3	< 1.56	1	1
0241+0023	02 41 10.0	+00 23 01.4	0.790	20.47	4011	9.33	15.8	5.0	2.35 ± 0.57	1	1
0244-0134	02 44 01.9	-01 34 03.0	4.053	18.4	875	0.64	17.6	7.4	0.55 ± 0.15	2	6
0248+1802	02 48 54.3	+18 02 49.9	4.430	18.4	876	0.66	18.1	1.7	3.55 ± 0.83	2	5
0259+0048	02 59 59.7	+00 48 13.6	0.892	19.44	4145	0.54	40.6	4.7	3.13 ± 0.47	1	1
0311-1722	03 11 15.2	-17 22 47.3	4.000	18.0	3154	0.57	8.9	6.1	< 1.07	3	3
0314-0111	03 14 27.5	-01 11 52.3	0.387	18.05	4084	4.48	114.8	1.9	23.9 ± 5.29	1	1
0403-1703	04 03 56.6	-17 03 24.1	4.236	18.7	2182	0.59	13.9	3.8	1.08 ± 0.29	2	6
0419-5716	04 19 50.9	-57 16 13.1	4.460	18.7	4066	0.58	9.3	4.0	0.71 ± 0.24	3	3
0755+2203	07 55 02.1	+22 03 46.9	0.399	18.99	647, 3767	3.85, 7.26	457.0	156.2	5.83 ± 0.41	1	1
0755+4058	07 55 35.6	+40 58 03.0	2.417	18.85	3032	9.48	15.6	7.3	1.37 ± 0.36	1	1
0755+4111	07 55 40.0	+41 11 19.1	0.967	17.86	3032	10.0	9.6	7.3	1.13 ± 0.35	1	1
0755+4056	07 55 45.6	+40 56 43.6	2.348	19.17	3032	9.06	19.8	7.3	1.49 ± 0.37	1	1
0819+3649	08 19 51.4	+36 49 50.8	0.736	19.19	4119	11.5	86.6	7.3	11.22 ± 2.71	1	1
0832+5243	08 32 06.0	+52 43 59.3	1.572	19.47	1643	3.80	7.6	9.1	< 0.56	1	1
0845+3431	08 45 26.6	+34 31 02.0	2.046	19.88	818	10.1	3.4	4.5	< 2.13	1	1
0849+4457	08 49 05.1	+44 57 14.8	1.259	20.00	927, 1708	3.26, 3.26	938.2	186.5	2.37 ± 0.11	1	1
0849+4500	08 49 43.7	+45 00 24.3	1.592	18.39	927, 1708	10.4, 10.4	1149.6	186.5	3.87 ± 0.13	1	1
0910+5427	09 10 29.0	+54 27 19.0	0.525	18.76	2227	7.57	3327.4	105.7	19.95 ± 0.74	1	1
0912+0547	09 12 10.3	+05 47 42.1	3.240	18.06	419, 1629	10.9, 11.0	53.9	38.6	0.88 ± 0.14	1	1
0918+5139	09 18 28.6	+51 39 32.1	0.185	17.46	533	4.51	147.5	11.3	5.05 ± 3.14	1	1
0918+0647	09 18 47.5	+06 47 04.7	0.821	18.80	3563	11.1	78.0	4.9	5.62 ± 1.63	1	1
0933+5515	09 33 59.3	+55 15 50.8	1.863	19.08	805	1.27	779.7	40.8	4.57 ± 0.24	1	1
0941+5948	09 41 33.7	+59 48 11.3	0.967	16.38	3035	2.83	398.1	4.2	25.16 ± 2.86	1	1
0950+5619	09 50 24.0	+56 19 46.7	1.912	20.53	4151	6.76	29.0	8.9	1.87 ± 0.34	1	1
0951+5940	09 51 30.2	+59 40 37.1	1.056	18.74	3036	5.39	45.9	5.1	4.48 ± 0.66	1	1
0951+5944	09 51 51.6	+59 44 30.0	2.338	19.79	3036	1.12	28.5	5.1	1.26 ± 0.28	1	1
0952+5152	09 52 40.2	+51 52 50.0	0.553	18.47	3195	2.42	1487.6	26.9	12.81 ± 0.94	1	1
0952+5151	09 52 43.0	+51 51 21.1	0.861	17.34	3195	3.25	1688.2	26.9	14.79 ± 0.76	1	1
0955+5935	09 55 05.6	+59 35 17.6	0.912	18.91	3156	4.84	38.3	5.7	3.50 ± 0.56	1	1
0955+5940	09 55 11.3	+59 40 32.2	4.340	18.58	3156	0.60	17.8	5.7	0.90 ± 0.21	1	1
0955+4116	09 55 42.1	+41 16 55.3	3.420	19.36	5294	7.45	31.2	17.3	1.01 ± 0.20	1	1
0955+4109	09 55 48.1	+41 09 55.3	2.307	18.74	5294	2.67	71.9	17.3	2.47 ± 0.30	1	1
0956+4110	09 56 40.4	+41 10 43.5	1.887	20.49	5294	7.23	12.8	17.3	0.58 ± 0.15	1	1
0958+0734	09 58 20.5	+07 34 36.1	1.885	18.44	2990	9.38	296.9	14.1	14.01 ± 1.66	1	1
0958+0747	09 58 22.6	+07 47 47.7	3.218	20.07	2990	8.48	10.6	14.1	0.72 ± 0.20	1	1
0958+0745	09 58 36.6	+07 45 56.3	1.487	19.17	2990	6.23	192.1	14.1	4.70 ± 0.63	1	1

Table 2—Continued

Source	RA J2000	DEC J2000	z	r^a	OBSID	θ^b	Counts ^c	Exp. Time ksec	f_X^d 10^{-14} ergs cm^{-2} s^{-1}	Spec. Ref. ^e	Phot. Ref. ^f
1002+5542	10 02 05.4	+55 42 57.9	1.151	18.03	2038	2.84	161.6	26.6	3.44 ± 0.62	1	1
1003+4736	10 03 52.8	+47 36 53.4	2.934	19.72	4152	0.59	64.5	13.7	1.24 ± 0.16	1	1
1013-0052	10 13 14.9	-00 52 33.6	0.275	17.78	4085	4.49	192.3	2.0	32.75 ± 5.50	1	1
1019+4737	10 19 02.0	+47 37 14.6	2.944	19.19	4153	0.58	28.7	8.0	0.98 ± 0.19	1	1
1023+0415	10 23 50.9	+04 15 42.0	1.809	19.40	1651, 909	6.66, 6.66	240.7	211.7	2.19 ± 0.14	1	1
1030+0524	10 30 31.6	+05 24 54.9	1.182	17.74	3357	0.88	11.2	8.0	0.57 ± 0.15	1	1
1032+5738	10 32 27.9	+57 38 22.5	1.968	20.58	3345, 3344	8.17, 8.18	589.7	77.0	3.79 ± 0.16	1	1
1032+5800	10 32 36.2	+58 00 34.0	0.686	19.83	3343	7.90	1.7	37.0	< 0.25	1	1
1036-0343	10 36 23.8	-03 43 20.0	4.509	18.5	877	0.65	15.7	3.4	1.29 ± 0.33	2	6
1038+4727	10 38 08.7	+47 27 34.9	1.047	18.56	4154	3.96	15.6	9.8	0.65 ± 0.17	1	1
1042+0100	10 42 30.7	+01 00 01.6	1.400	18.40	4086	4.87	21.2	1.7	4.05 ± 1.27	1	1
1044+5921	10 44 54.9	+59 21 34.1	1.291	19.03	5030	7.31	265.5	65.7	2.51 ± 0.27	1	1
1049+5750	10 49 21.5	+57 50 36.6	1.106	18.81	1673	8.73	23.9	4.9	2.92 ± 0.62	1	1
1050+5702	10 50 15.6	+57 02 55.7	3.273	20.17	1679, 1680	10.9, 8.19	24.0	9.4	1.47 ± 0.33	1	1
1050+5738	10 50 50.1	+57 38 20.0	1.281	19.09	1678	3.98	32.8	4.7	3.49 ± 0.62	1	1
1052+5724	10 52 39.6	+57 24 31.4	1.111	17.79	1683	2.96	90.8	4.7	8.81 ± 1.64	1	1
1053+5735	10 53 16.8	+57 35 50.8	1.204	19.08	1683, 1684	9.42, 7.40	161.8	9.4	10.6 ± 0.96	1	1
1054+5740	10 54 04.1	+57 40 19.8	1.100	18.04	1688	5.25	24.7	4.7	2.61 ± 0.54	1	1
1054+5720	10 54 22.6	+57 20 31.0	2.972	19.85	1687	7.13	3.1	4.7	< 1.99	1	1
1055+5704	10 55 18.1	+57 04 23.6	0.695	18.73	1686, 1691	8.96, 8.35	86.7	9.4	6.43 ± 1.06	1	1
1056+5722	10 56 44.5	+57 22 33.5	0.286	18.90	1693	4.96	26.2	5.7	2.56 ± 0.52	1	1
1057+4555	10 57 56.4	+45 55 52.0	4.100	17.48	878	0.65	34.8	2.8	3.12 ± 0.53	2	1
1109+0900	11 09 05.3	+09 00 48.7	1.674	19.42	3252	7.34	22.1	10.0	1.40 ± 0.31	1	1
1111+5532	11 11 32.1	+55 32 40.3	1.004	18.44	2025	7.89	333.8	59.4	3.70 ± 0.37	1	1
1114+5315	11 14 52.8	+53 15 31.7	1.213	19.02	3253, 3321	4.01, 8.41	39.8	13.6	4.60 ± 0.46	1	1
1115+5309	11 15 20.7	+53 09 22.1	0.877	18.05	3321	1.18	2.6	4.8	< 0.55	1	1
1129-0137	11 29 43.9	-01 37 52.3	1.294	18.15	2082	5.66	128.7	4.8	7.96 ± 1.14	1	1
1129-0150	11 29 51.2	-01 50 37.3	1.784	20.24	2082	7.89	23.7	4.8	2.86 ± 0.56	1	1
1136+0159	11 36 21.2	+01 59 27.9	0.766	19.24	4833	3.15	85.1	5.9	5.28 ± 0.98	1	1
1136+0158	11 36 31.9	+01 58 01.1	1.470	17.85	4833	0.57	9.8	5.9	0.74 ± 0.21	1	1
1136+0207	11 36 33.1	+02 07 47.7	0.239	18.07	4833	9.31	65.4	5.9	5.48 ± 2.06	1	1
1202-0129	12 02 26.8	-01 29 15.3	0.150	17.13	4108	0.59	2361.2	9.4	54.36 ± 3.27	1	1
1204+0150	12 04 36.6	+01 50 25.6	1.927	18.63	3234	5.49	148.6	30.0	1.85 ± 0.19	1	1
1208+0016	12 08 29.6	+00 16 42.7	1.063	18.97	2083	5.86	34.8	4.6	3.53 ± 0.61	1	1
1213+0252	12 13 43.0	+02 52 48.9	0.641	19.30	4110	4.55	57.9	10.0	1.69 ± 0.47	1	1
1214+0055	12 14 15.2	+00 55 11.5	0.395	18.35	4087	4.48	137.3	2.0	21.42 ± 3.75	1	1
1215-0034	12 15 40.5	-00 34 33.8	0.757	19.46	4201	3.45	551.2	44.5	7.16 ± 0.56	1	1
1218+0546	12 18 36.1	+05 46 28.1	0.795	18.89	3322	0.98	72.5	4.6	3.53 ± 0.60	1	1
1220-0025	12 20 04.4	-00 25 39.1	0.421	18.96	3141	0.58	2380.4	19.7	30.45 ± 1.26	1	1
1223+1034	12 23 07.5	+10 34 48.2	2.747	18.59	3232	4.65	302.6	30.1	3.02 ± 0.20	1	1
1226-0011	12 26 52.0	-00 11 59.6	1.175	17.88	4865	0.58	137.7	4.9	8.07 ± 1.05	1	1
1228+4413	12 28 18.0	+44 13 02.0	0.662	18.05	2031	5.81	3.0	26.6	< 0.27	1	1
1228+4411	12 28 53.7	+44 11 52.9	1.276	18.79	2031	9.09	96.6	26.6	2.71 ± 0.30	1	1
1230+0302	12 30 05.8	+03 02 04.2	1.604	18.91	4040	3.01	34.1	3.5	3.07 ± 0.56	1	1
1230+0305	12 30 25.9	+03 05 35.4	1.055	19.45	4040	3.17	35.9	3.5	4.72 ± 0.80	1	1
1230+0306	12 30 27.4	+03 06 27.5	0.628	18.65	4040	4.05	105.6	3.5	14.99 ± 2.32	1	1
1230+0308	12 30 39.9	+03 08 57.3	1.843	19.50	4040	8.02	12.7	3.5	1.73 ± 0.54	1	1
1230+0305	12 30 54.7	+03 05 37.2	0.427	19.19	4040	9.76	16.8	3.5	3.05 ± 0.78	1	1
1236+6215	12 36 22.9	+62 15 26.6	2.587	20.44	580, 2423, 2344, 3409, 967, 966, 3389, 957, 3408, 2233, 2232, 2386, 3388, 2421, 2234, 3293, 3294, 3390, 3391, 1671	6.83, 1.67, 5.38, 1.79, 5.46, 5.45, 4.11, 1.73, 4.12, 1.67, 1.69, 5.38, 4.12, 1.64, 1.64, 4.12, 1.79, 1.79, 1.79, 5.37	3741.3	1961.0	0.90 ± 0.02	1	1
1237+6203	12 37 16.0	+62 03 23.4	2.068	19.86	580, 2344, 967, 966, 2386, 1671	9.23, 9.77, 9.59, 9.62, 9.78, 9.78	198.9	431.9	0.30 ± 0.03	1	1
1242+0249	12 42 55.3	+02 49 57.0	1.458	19.21	323, 3926	8.17, 6.56	657.2	127.1	3.250 ± 0.17	1	1
1245-0027	12 45 41.0	-00 27 44.9	1.693	18.58	4018	7.82	88.7	4.9	11.24 ± 1.21	1	1
1255+5652	12 55 35.1	+56 52 39.6	1.803	19.13	1031	6.00	339.3	39.3	1.79 ± 0.18	1	1
1255+5650	12 55 36.2	+56 50 00.1	1.373	19.83	1031	6.32	0.0	39.3	< 0.14	1	1
1258-0143	12 58 49.8	-01 43 03.3	0.967	17.06	4178	4.58	2024.9	27.3	21.09 ± 1.00	1	1

Table 2—Continued

Source	RA J2000	DEC J2000	z	r^a	OBSID	θ^b	Counts ^c	Exp. Time ksec	f_X^d 10^{-14} ergs cm^{-2} s^{-1}	Spec. Ref. ^e	Phot. Ref. ^f
1259+0102	12 59 43.6	+01 02 55.0	0.394	18.34	4088	4.48	4.0	1.9	< 2.47	1	1
1311+0031	13 11 08.5	+00 31 51.7	0.429	17.92	4089	4.48	14.9	1.7	2.86 ± 0.76	1	1
1317+3531	13 17 43.2	+35 31 31.1	4.360	19.1	879	0.64	5.7	2.8	< 1.78	2	5
1344-0000	13 44 25.9	-00 00 56.2	1.095	18.58	2251	0.39	26.2	9.6	0.82 ± 0.16	1	1
1411+5217	14 11 04.1	+52 17 55.6	2.882	19.07	2254	6.15	247.3	90.9	1.48 ± 0.11	1	1
1411+5205	14 11 04.9	+52 05 16.8	1.083	18.97	2254	7.19	41.1	90.9	1.20 ± 0.68	1	1
1417+4456	14 17 00.8	+44 56 06.4	0.113	16.32	541	8.26	5313.3	31.2	92.89 ± 4.08	1	1
1419+4709	14 19 51.9	+47 09 01.4	2.288	17.37	3076	0.59	174.3	7.7	6.77 ± 0.53	1	1
1424+4214	14 24 14.1	+42 14 00.1	1.608	19.03	3077	5.91	133.1	5.9	6.81 ± 0.79	1	1
1424+4210	14 24 36.0	+42 10 30.5	2.217	17.51	3077	0.58	137.0	5.9	5.35 ± 0.57	1	1
1432-0059	14 32 44.4	-00 59 15.2	1.026	17.26	907	7.56	1715.9	21.4	43.53 ± 2.13	1	1
1433+0227	14 33 35.3	+02 27 18.3	2.072	19.94	3959	3.85	17.0	3.5	2.57 ± 0.63	1	1
1434+0227	14 34 07.5	+02 27 04.6	1.710	19.41	3959	4.24	28.4	3.5	2.91 ± 0.56	1	1
1438+0341	14 38 42.0	+03 41 10.4	1.737	18.27	3290	5.97	296.9	57.6	3.11 ± 0.20	1	1
1438+0335	14 38 59.1	+03 35 47.5	0.733	18.43	3290	8.23	498.2	57.6	7.25 ± 0.50	1	1
1442+0110	14 42 31.7	+01 10 55.3	4.560	20.90	3960	0.58	43.9	11.0	1.37 ± 0.20	4	1
1443+5856	14 43 40.8	+58 56 53.2	4.260	18.28	3160	0.58	16.3	5.8	0.71 ± 0.19	1	1
1445+0129	14 45 54.8	+01 29 03.3	1.845	20.00	2112	2.40	38.9	5.9	2.22 ± 0.34	1	1
1448+4738	14 48 53.4	+47 38 21.3	2.894	19.39	4155	0.58	19.0	6.9	0.93 ± 0.21	1	1
1448+0015	14 48 56.7	+00 15 10.3	0.832	18.80	4092	7.59	19.2	2.1	4.64 ± 1.08	1	1
1449+0024	14 49 13.5	+00 24 06.9	0.440	19.13	4092	3.10	48.0	2.1	7.82 ± 1.18	1	1
1452+4304	14 52 15.6	+43 04 48.7	0.296	18.89	1048, 2424	3.14, 3.11	785.1	47.2	5.010 ± 0.49	1	1
1452+4308	14 52 40.9	+43 08 14.4	1.704	19.41	1048	8.36	139.8	17.7	4.46 ± 0.38	1	1
1511+5659	15 11 26.5	+56 59 34.8	1.031	17.55	3334	9.81	3.9	4.9	< 4.30	1	1
1515+5521	15 15 04.9	+55 21 07.3	1.844	20.40	3006	9.83	18.2	9.6	1.02 ± 0.39	1	1
1539+4313	15 39 47.6	+43 13 41.6	0.347	18.75	2993	1.30	870.1	14.8	15.96 ± 1.28	1	1
1543+5405	15 43 16.4	+54 05 26.1	0.245	18.11	822	8.39	132.3	4.5	14.35 ± 3.03	1	1
1545+4846	15 45 30.2	+48 46 09.1	0.399	16.44	3339	8.93	245.8	4.9	34.29 ± 5.79	1	1
1605-0109	16 05 17.8	-01 09 55.5	1.572	19.14	2086	5.42	80.4	4.6	7.08 ± 0.91	1	1
1618+3456	16 18 34.0	+34 56 25.6	1.922	18.73	3341	5.29	17.4	4.9	1.83 ± 0.46	1	1
1640+4644	16 40 25.0	+46 44 49.1	0.537	18.38	896	1.17	1049.2	42.3	5.17 ± 0.41	1	1
1641+4649	16 41 10.6	+46 49 11.9	0.695	19.21	896	9.98	366.1	42.3	4.83 ± 0.48	1	1
1641+4000	16 41 54.2	+40 00 33.1	1.002	17.81	3575	1.29	311.8	46.5	3.09 ± 0.38	1	1
1657+3524	16 57 13.2	+35 24 39.4	2.328	19.37	3662	8.88	102.8	49.6	1.16 ± 0.14	1	1
1701+6412	17 01 00.6	+64 12 09.0	2.735	16.00	547	4.98	364.7	49.5	3.69 ± 0.21	1	1
1702+3405	17 02 24.5	+34 05 39.0	2.038	18.93	4179	5.25	97.8	57.0	0.65 ± 0.06	1	1
1703+6045	17 03 55.8	+60 45 11.7	0.284	18.77	435	4.97	250.3	9.1	12.0 ± 2.11	1	1
1708+6154	17 08 17.9	+61 54 48.6	1.414	17.84	4864	0.58	239.4	4.1	16.4 ± 1.83	1	1
1719+2732	17 19 27.3	+27 32 46.8	1.446	18.72	3245	10.1	92.7	10.0	7.27 ± 1.29	1	1
1720+2638	17 20 26.5	+26 38 16.0	1.141	19.13	3224, 4361	4.43, 5.43	170.6	49.5	2.66 ± 0.27	1	1
1735+5355	17 35 51.9	+53 55 15.7	0.955	17.91	4863	0.58	268.2	5.4	14.86 ± 1.76	1	1
1737+5828	17 37 16.6	+58 28 39.5	1.775	19.05	3038	3.28	21.2	4.6	3.71 ± 0.83	1	1
1738+5837	17 38 36.2	+58 37 48.6	1.279	17.71	4860	0.58	10.1	3.9	0.76 ± 0.26	1	1
2215-1611	22 15 27.1	-16 11 33.0	3.990	18.1	2185	0.59	16.6	3.2	1.35 ± 0.37	2	6
2238-0921	22 38 19.8	-09 21 06.0	3.259	18.04	2411	6.07	1.3	5.9	< 5.97	1	1
2238-0937	22 38 54.7	-09 37 36.2	1.472	19.14	2411	12.7	4.0	5.8	< 17.5	1	1
2239-0933	22 39 17.3	-09 33 40.9	1.817	19.28	2414	11.3	9.9	5.7	< 14.6	1	1
2249-0808	22 49 03.3	-08 08 41.7	0.457	19.42	583	8.04	304.5	11.7	13.6 ± 1.97	1	1
2337+0025	23 37 18.1	+00 25 50.7	2.053	19.28	3328	7.59	20.6	9.2	1.85 ± 0.40	1	1
2337+0022	23 37 22.0	+00 22 38.9	1.376	19.27	3248	4.50	8.0	9.2	0.97 ± 0.33	1	1
2337+0026	23 37 39.1	+00 26 56.2	1.703	18.85	3248	7.44	61.7	9.2	4.13 ± 0.58	1	1
2348+0107	23 48 40.1	+01 07 53.5	0.718	18.50	861	10.8	779.4	74.2	7.08 ± 0.46	1	1

Note. — For sources with multiple observation IDs, the off-axis angles are reported for each. However, the reported counts and exposure time are summed over the observation IDs.

^a r -band apparent magnitude.

^bOff-axis angle, in arcmin.

^cNumber of observed background-subtracted source counts in the range 0.3–7.0 keV.

^dUnabsorbed 2–10 keV flux, assuming a power-law. A photon index of $\Gamma_{\mathcal{X}} = 1.9$ was assumed for those sources with < 50 counts. A “ $<$ ” denotes an upper limit.

^eReference for the observed frame optical spectrum.

^fReference for the r -band magnitude.

References. — (1) SDSS; (2) Constantin et al. (2002); (3) Péroux et al. (2001); (4) Anderson et al. (2001); (5) Kennefick et al. (1995); (6) Storrie-Lombardi et al. (1996)

Table 3. Continuum and Fe Emission Fitting Windows

	1	2	3	4	5	6
UV	$\lambda\lambda 1350-1365$	$\lambda\lambda 1427-1500$	$\lambda\lambda 1760-1860$	$\lambda\lambda 1950-2300$	$\lambda\lambda 2470-2755$	$\lambda\lambda 2855-3010$
Optical	$\lambda\lambda 3535-3700$	$\lambda\lambda 4100-4200$	$\lambda\lambda 4400-4700$	$\lambda\lambda 5100-6200$	$\lambda\lambda 6800-7534$...

Table 4. X-ray and UV Parameters

Source	Redshift	Gal. N_H^a 10^{20} cm^{-2}	n_0^b $10^{-6} \text{ cm}^{-2} \text{ s}^{-1} \text{ keV}^{-1}$	Γ_X^c	$\log \nu L_\nu(2500\text{\AA})$ ergs s^{-1}	$\log \nu L_\nu(2 \text{ keV})$ ergs s^{-1}	α_{ox}	α_{UV}^d
0002+0049	1.353	2.82	41.87 ± 3.08	2.20 ± 0.11	45.87	44.88	1.38	1.33
0006-0015	1.725	3.16	13.26 ^{+2.04} _{-1.85}	1.81 ^{+0.22} _{-0.22}	46.12	44.61	1.58	0.74
0022+0016	0.575	2.70	11.40 ± 0.88	2.30 ± 0.20	44.97	43.35	1.62	0.52
0027+0026	0.205	3.01	47.63 ± 7.30	1.68 ± 0.27	43.90	43.04	1.33	...
0031+0034	1.735	2.41	12.24 ± 1.49	2.21 ± 0.18	45.98	44.62	1.52	0.15
0050-0053 ^e	4.332	2.70	2.66 ^{+0.56} _{-0.50}	2.02 ^{+0.33} _{-0.32}	46.54	44.84	1.65	0.98
0057+1450	0.624	4.35	< 3.69	...	45.11	< 42.99	> 1.81	0.64
0059+0003	4.178	3.01	4.65 ^{+1.62} _{-1.33}	0.91 ^{+0.44} _{-0.44}	46.58	45.05	1.59	1.12
0106+0048	4.437	3.16	7.85 ^{+1.70} _{-1.49}	1.95 ^{+0.31} _{-0.30}	46.83	45.33	1.57	0.60
0113+1531	0.576	4.40	50.18 ± 3.63	1.91 ± 0.08	45.05	44.04	1.39	0.53
0113+1535	1.807	4.38	24.49 ± 1.37	2.29 ± 0.10	46.17	44.98	1.46	0.53
0115+0020	1.276	3.34	26.95 ± 1.77	1.92 ± 0.11	45.55	44.61	1.36	0.64
0133+0400	4.150	3.01	7.84 ^{+1.34} _{-1.21}	2.16 ^{+0.28} _{-0.27}	46.98	45.27	1.66	1.00
0134+3307	4.530	4.67	5.29 ^{+1.31} _{-1.14}	2.24 ^{+0.42} _{-0.40}	47.11	45.18	1.74	0.65
0148+0001	1.705	2.88	14.12 ^{+2.29} _{-2.07}	2.39 ^{+0.24} _{-0.24}	46.29	44.62	1.64	0.16
0148-0002	0.930	2.75	31.91 ± 3.49	2.31 ± 0.19	45.40	44.34	1.40	0.54
0152+0105	0.647	2.80	27.70 ± 2.75	2.50 ± 0.18	44.90	43.85	1.40	0.18
0153+0052	1.161	2.69	9.06 ± 1.44	2.19 ± 0.26	45.49	44.05	1.56	0.59
0156+0053	1.652	2.69	18.15 ± 2.12	1.36 ± 0.15	46.01	44.63	1.53	1.38
0159+0023	0.163	2.13	775.4 ± 12.4	2.39 ± 0.03	44.90	43.86	1.40	...
0201-0919	0.661	2.08	46.05 ± 2.87	2.16 ± 0.12	45.40	44.12	1.49	0.90
0208+0022	1.885	2.78	18.49 ± 2.65	1.56 ± 0.20	46.69	44.79	1.73	0.49
0209+0517	4.140	4.57	6.39 ^{+1.27} _{-1.12}	2.72 ^{+0.33} _{-0.31}	47.20	45.18	1.78	0.68
0232-0731	1.164	3.30	< 7.39	...	45.24	< 43.95	> 1.50	1.41
0241-0811	0.979	2.90	< 6.24	...	44.87	> 43.70	> 1.45	0.63
0241+0023	0.790	3.37	9.46 ^{+2.45} _{-2.12}	2.01 ^{+0.48} _{-0.44}	44.55	43.64	1.35	0.78
0244-0134	4.053	3.52	2.14 ^{+0.62} _{-0.53}	1.52 ^{+0.41} _{-0.39}	47.22	44.68	1.97	1.06
0248+1802	4.430	9.02	13.64 ^{+3.43} _{-2.94}	1.97 ^{+0.39} _{-0.37}	46.97	45.57	1.54	0.34
0259+0048	0.892	7.22	12.56 ^{+2.18} _{-1.94}	1.02 ^{+1.0} _{-1.02}	45.11	43.90	1.46	0.58
0311-1722	4.000	3.81	< 4.14	...	47.21	< 44.95	> 1.87	1.90
0314-0111	0.387	5.78	97.12 ± 9.62	2.75 ± 0.17	44.88	43.79	1.42	...
0403-1703	4.236	2.29	4.16 ^{+1.20} _{-1.01}	1.39 ^{+0.37} _{-0.37}	46.62	45.01	1.62	1.26
0419-5716	4.460	1.67	2.73 ^{+1.01} _{-0.82}	2.13 ^{+0.51} _{-0.49}	47.20	44.88	1.89	2.18
0755+2203	0.400	5.60	23.69 ± 2.84	1.38 ± 0.10	44.55	43.43	1.43	...
0755+4058	2.417	4.78	5.36 ^{+1.52} _{-1.31}	3.22 ^{+0.57} _{-0.55}	46.16	44.56	1.62	0.27
0755+4111	0.967	4.98	4.53 ^{+1.51} _{-1.27}	2.09 ^{+0.61} _{-0.55}	45.78	43.54	1.86	0.20
0755+4056	2.348	4.73	5.86 ^{+1.55} _{-1.34}	2.75 ^{+0.56} _{-0.53}	46.03	44.57	1.56	0.45
0819+3649	0.736	4.82	45.20 ± 5.24	3.08 ± 0.26	45.00	44.18	1.32	0.38
0832+5243	1.573	3.87	< 2.23	...	45.58	< 43.74	> 1.71	0.30
0845+3431	2.046	3.41	< 8.40	...	45.60	< 44.59	> 1.39	0.62
0849+4457	1.259	2.75	9.43 ± 0.37	2.07 ± 0.07	45.08	44.15	1.36	0.38
0849+4500	1.592	2.70	15.33 ± 0.57	2.10 ± 0.06	45.94	44.61	1.51	0.53
0910+5427	0.526	2.03	80.75 ± 1.73	2.11 ± 0.04	44.85	44.13	1.28	-0.3
0912+0547	3.241	3.65	3.40 ± 0.56	1.94 ± 0.31	46.75	44.67	1.80	0.67
0914+5613 ^e	4.035	2.89	0.69 ^{+0.24} _{-0.20}	1.04 ^{+0.55} _{-0.52}	46.14	44.18	1.75	1.43
0918+5139	0.185	1.36	20.66 ± 9.26	0.92 ± 0.33	44.15	42.75	1.54	...
0918+0647	0.821	3.65	22.58 ± 3.32	2.81 ± 0.28	45.21	44.03	1.45	0.68
0933+5515	1.864	2.00	18.05 ± 1.18	2.08 ± 0.11	45.83	44.85	1.37	0.81
0941+5948	0.968	2.19	100.8 ± 5.90	2.44 ± 0.12	46.28	44.89	1.54	0.48
0950+5619	1.913	1.19	7.36 ^{+1.40} _{-1.25}	2.87 ^{+0.38} _{-0.36}	45.20	44.46	1.28	0.68
0951+5940	1.057	1.67	17.92 ^{+2.76} _{-2.51}	1.80 ^{+0.25} _{-0.24}	45.43	44.23	1.46	0.55
0951+5944	2.339	1.51	4.95 ^{+1.17} _{-1.01}	2.01 ^{+0.38} _{-0.36}	45.60	44.49	1.43	0.21
0952+5152	0.554	0.88	51.81 ± 1.52	2.29 ± 0.06	44.97	43.97	1.38	0.60
0952+5151	0.862	0.86	59.38 ± 1.62	2.16 ± 0.05	45.59	44.53	1.41	0.88

Table 4—Continued

Source	Redshift	Gal. N_H^a 10^{20} cm^{-2}	n_0^b $10^{-6} \text{ cm}^{-2} \text{ s}^{-1} \text{ keV}^{-1}$	Γ_X^c	$\log \nu L_\nu(2500 \text{ \AA})$ ergs s^{-1}	$\log \nu L_\nu(2 \text{ keV})$ ergs s^{-1}	α_{ox}	α_{UV}^d
0955+5935	0.912	1.50	$14.05^{+2.37}_{-2.13}$	$2.20^{+0.30}_{-0.30}$	45.08	43.97	1.42	0.69
0955+5940	4.340	1.33	$3.47^{+0.89}_{-0.76}$	$1.87^{+0.34}_{-0.33}$	46.76	44.96	1.69	0.47
0955+4116	3.420	0.64	$3.93^{+0.83}_{-0.73}$	$2.15^{+0.38}_{-0.36}$	46.16	44.78	1.53	0.23
0955+4109	2.308	0.59	9.68 ± 1.36	2.13 ± 0.22	46.09	44.82	1.49	0.25
0956+4110	1.887	0.72	$2.28^{+0.63}_{-0.54}$	$2.50^{+0.53}_{-0.50}$	45.28	43.94	1.51	-0.5
0958+0734	1.885	2.95	59.53 ± 11.9	2.22 ± 0.26	46.10	45.40	1.27	0.72
0958+0747	3.219	2.97	$2.77^{+0.82}_{-0.70}$	$2.56^{+0.57}_{-0.54}$	45.82	44.56	1.48	0.44
0958+0745	1.488	3.05	18.66 ± 1.47	2.20 ± 0.19	45.46	44.64	1.31	0.72
1002+5542	1.151	0.84	13.75 ± 2.00	1.27 ± 0.15	45.76	44.19	1.60	1.04
1003+4736	2.934	0.93	4.83 ± 0.64	1.53 ± 0.17	45.88	44.60	1.49	0.52
1013-0052	0.276	3.49	133.5 ± 10.1	2.74 ± 0.12	44.55	43.56	1.38	...
1019+4737	2.945	0.99	$3.82^{+0.78}_{-0.69}$	$2.31^{+0.28}_{-0.27}$	46.04	44.61	1.55	0.53
1023+0415	1.809	2.89	8.66 ± 0.68	2.05 ± 0.11	45.65	44.50	1.45	0.55
1030+0524	1.183	2.72	$2.27^{+0.67}_{-0.56}$	$1.21^{+0.40}_{-0.39}$	45.85	43.46	1.92	0.48
1032+5738	1.969	0.59	14.95 ± 0.81	1.73 ± 0.07	45.15	44.77	1.15	0.73
1032+5800	0.687	0.61	< 1.00	...	44.55	< 42.52	> 1.78	0.57
1036-0343	4.509	4.77	$4.96^{+1.38}_{-1.18}$	$2.67^{+0.50}_{-0.45}$	47.09	45.15	1.74	0.62
1038+4727	1.047	1.47	$2.61^{+0.74}_{-0.64}$	$0.92^{+0.40}_{-0.40}$	45.55	43.39	1.83	0.69
1042+0100	1.401	3.95	$16.10^{+3.88}_{-3.36}$	$2.25^{+0.36}_{-0.35}$	45.85	44.51	1.51	0.61
1044+5921	1.292	0.70	10.00 ± 0.80	1.85 ± 0.11	45.45	44.19	1.48	0.41
1049+5750	1.106	0.60	$11.66^{+2.65}_{-2.31}$	$1.79^{+0.40}_{-0.38}$	45.42	44.10	1.51	0.72
1050+5702	3.273	0.59	$5.70^{+1.38}_{-1.20}$	$2.45^{+0.49}_{-0.46}$	45.92	44.89	1.40	0.81
1050+5738	1.281	0.59	$13.89^{+2.61}_{-2.32}$	$2.68^{+0.36}_{-0.35}$	45.38	44.33	1.41	0.53
1052+5724	1.112	0.60	35.22 ± 4.58	1.80 ± 0.18	45.76	44.58	1.45	0.72
1053+5735	1.205	0.59	42.26 ± 4.19	1.86 ± 0.15	45.29	44.74	1.21	1.37
1054+5740	1.101	0.59	$10.45^{+2.30}_{-2.01}$	$2.12^{+0.37}_{-0.36}$	45.72	44.04	1.64	0.54
1054+5720	2.972	0.59	< 7.75	...	45.91	< 44.93	> 1.38	0.62
1055+5704	0.696	0.60	25.93 ± 3.29	2.12 ± 0.20	44.92	43.93	1.38	0.87
1056+5722	0.286	0.60	$10.45^{+2.24}_{-1.97}$	$0.28^{+0.32}_{-0.33}$	44.01	42.66	1.52	...
1057+4555	4.100	1.16	$12.05^{+2.17}_{-1.94}$	$2.08^{+0.27}_{-0.27}$	47.67	45.44	1.86	2.14
1109+0900	1.674	2.79	$5.56^{+1.29}_{-1.13}$	$1.67^{+0.38}_{-0.36}$	45.60	44.20	1.54	0.85
1111+5532	1.004	0.78	14.82 ± 0.91	3.23 ± 0.10	45.50	44.10	1.54	0.71
1114+5315	1.213	0.96	18.34 ± 2.19	1.65 ± 0.16	45.29	44.38	1.35	2.11
1115+5309	0.877	0.97	< 2.21	...	45.53	< 43.13	> 1.92	0.56
1129-0137	1.295	3.58	31.69 ± 3.31	1.54 ± 0.15	45.71	44.67	1.40	0.75
1129-0150	1.785	3.56	$11.30^{+2.37}_{-2.09}$	$2.11^{+0.37}_{-0.35}$	45.15	44.57	1.22	0.97
1136+0159	0.766	2.50	21.23 ± 2.44	2.03 ± 0.19	44.94	43.96	1.38	0.73
1136+0158	1.471	2.61	$2.95^{+0.89}_{-0.75}$	$1.45^{+0.39}_{-0.40}$	46.10	43.80	1.88	0.57
1136+0207	0.239	2.61	22.37 ± 4.05	1.63 ± 0.26	44.04	42.87	1.45	...
1202-0129	0.150	2.22	222.5 ± 5.86	3.02 ± 0.04	44.05	43.09	1.37	...
1204+0150	1.927	1.88	7.29 ± 0.63	2.10 ± 0.15	45.93	44.50	1.55	0.29
1208+0016	1.063	1.99	$14.11^{+2.56}_{-2.29}$	$1.25^{+0.28}_{-0.27}$	45.21	44.14	1.41	0.92
1213+0252	0.641	1.74	6.82 ± 0.99	2.10 ± 0.25	44.64	43.27	1.53	0.98
1214+0055	0.396	1.95	87.02 ± 7.77	2.44 ± 0.13	44.67	43.82	1.33	...
1215-0034	0.758	2.07	28.80 ± 1.72	2.08 ± 0.11	44.69	44.07	1.24	0.86
1218+0546	0.795	1.57	14.21 ± 2.11	1.28 ± 0.20	44.88	43.86	1.39	1.73
1220-0025	0.421	2.02	123.6 ± 2.93	1.45 ± 0.03	44.36	44.18	1.07	...
1223+1034	2.747	2.13	11.80 ± 0.81	1.59 ± 0.11	46.35	44.95	1.54	0.27
1226-0011	1.175	1.93	32.20 ± 2.91	2.43 ± 0.13	45.79	44.62	1.45	1.28
1228+4413	0.662	1.45	< 1.07	...	45.29	< 42.51	> 2.07	0.59
1228+4411	1.277	1.34	10.81 ± 1.18	2.12 ± 0.18	45.61	44.21	1.54	0.12
1230+0302	1.605	1.80	$11.27^{+2.17}_{-1.93}$	$1.61^{+0.29}_{-0.28}$	45.72	44.48	1.48	0.40
1230+0305	1.056	1.83	$18.88^{+3.37}_{-3.02}$	$2.37^{+0.32}_{-0.31}$	45.08	44.26	1.32	0.46
1230+0306	0.628	1.81	59.90 ± 6.60	2.03 ± 0.17	44.99	44.20	1.30	0.33

Table 4—Continued

Source	Redshift	Gal. N_H^a 10^{20} cm^{-2}	n_0^b $10^{-6} \text{ cm}^{-2} \text{ s}^{-1} \text{ keV}^{-1}$	Γ_X^c	$\log \nu L_\nu(2500\text{\AA})$ ergs s^{-1}	$\log \nu L_\nu(2 \text{ keV})$ ergs s^{-1}	α_{ox}	α_{UV}^d
1230+0308	1.843	1.81	$6.85^{+2.35}_{-1.92}$	$2.61^{+0.59}_{-0.57}$	45.63	44.39	1.48	0.29
1230+0305	0.428	1.83	$12.38^{+3.41}_{-2.92}$	$1.73^{+0.52}_{-0.48}$	44.28	43.13	1.44	...
1236+6215	2.587	1.52	1.19 ± 0.12	1.79 ± 0.19	45.53	43.95	1.61	0.55
1237+6203	2.068	1.44	3.54 ± 0.08	1.85 ± 0.03	45.66	44.21	1.56	1.02
1242+0249	1.459	1.92	12.89 ± 0.58	2.32 ± 0.08	45.58	44.47	1.43	0.06
1245-0027	1.693	1.73	44.48 ± 6.08	1.80 ± 0.19	45.96	45.10	1.33	0.72
1255+5652	1.804	1.25	7.06 ± 0.48	2.44 ± 0.11	45.74	44.46	1.49	0.34
1255+5650	1.374	1.25	< 0.56	...	45.23	< 43.00	> 1.85	0.28
1258-0143	0.967	1.54	84.49 ± 2.06	2.30 ± 0.05	46.03	44.81	1.47	0.56
1259+0102	0.395	1.62	< 10.05	...	44.48	< 42.96	> 1.58	...
1311+0031	0.429	1.84	$11.60^{+3.33}_{-2.80}$	$2.58^{+0.46}_{-0.44}$	44.82	43.11	1.66	...
1317+3531	4.360	0.99	< 6.84	...	46.54	< 45.26	> 1.49	0.90
1321+0038 ^e	4.716	1.88	$1.49^{+0.36}_{-0.31}$	$2.50^{+0.38}_{-0.37}$	46.60	44.67	1.74	2.04
1344-0000	1.096	1.89	$3.27^{+0.68}_{-0.60}$	$1.80^{+0.32}_{-0.30}$	45.47	43.53	1.74	0.43
1411+5217	2.883	1.33	5.79 ± 0.50	1.82 ± 0.14	46.16	44.75	1.54	0.57
1411+5205	1.084	1.40	4.80 ± 0.27	2.44 ± 0.49	45.30	43.70	1.61	0.73
1413+0000 ^e	4.078	3.15	$1.67^{+0.42}_{-0.37}$	$1.93^{+0.43}_{-0.39}$	46.46	44.58	1.72	1.66
1417+4456	0.114	1.13	380.7 ± 5.53	2.38 ± 0.03	44.11	43.21	1.35	...
1419+4709	2.288	1.56	26.56 ± 2.06	1.85 ± 0.12	46.83	45.19	1.63	1.25
1424+4214	1.608	1.25	26.00 ± 2.42	1.97 ± 0.15	45.63	44.84	1.30	-0.0
1424+4210	2.218	1.25	23.20 ± 2.15	2.39 ± 0.12	46.55	45.21	1.51	0.35
1432-0059	1.027	3.39	174.2 ± 5.15	2.06 ± 0.05	45.88	45.19	1.26	0.78
1433+0227	2.072	2.75	$9.59^{+2.54}_{-2.16}$	$2.36^{+0.46}_{-0.44}$	45.54	44.66	1.34	0.75
1434+0227	1.711	2.76	$10.73^{+2.19}_{-1.94}$	$2.05^{+0.32}_{-0.32}$	45.60	44.51	1.42	0.08
1438+0341	1.737	2.62	12.71 ± 0.93	2.11 ± 0.13	46.15	44.63	1.59	1.22
1438+0335	0.734	2.62	20.96 ± 3.70	1.70 ± 0.17	45.18	43.92	1.48	0.88
1442+0110	4.560	3.36	$5.25^{+0.82}_{-0.74}$	$1.98^{+0.23}_{-0.23}$	46.38	45.19	1.46	0.71
1443+5856	4.260	1.56	$2.74^{+0.80}_{-0.67}$	$2.29^{+0.42}_{-0.40}$	46.97	44.84	1.82	0.29
1444-0123 ^e	4.179	4.03	$1.59^{+0.53}_{-0.44}$	$2.95^{+0.77}_{-0.66}$	46.63	44.58	1.79	1.60
1445+0129	1.846	3.48	$8.75^{+1.42}_{-1.28}$	$2.45^{+0.29}_{-0.28}$	45.61	44.50	1.43	0.17
1448+4738	2.894	2.05	$3.61^{+0.86}_{-0.74}$	$1.72^{+0.32}_{-0.31}$	46.29	44.57	1.66	1.12
1448+0015	0.832	3.58	$18.64^{+4.73}_{-4.05}$	$2.24^{+0.48}_{-0.45}$	45.17	44.00	1.45	0.60
1449+0024	0.441	3.58	$31.72^{+5.06}_{-4.58}$	$2.50^{+0.27}_{-0.27}$	44.55	43.57	1.38	...
1452+4304	0.296	1.69	20.43 ± 0.99	1.97 ± 0.07	44.07	42.97	1.42	...
1452+4308	1.704	1.64	17.64 ± 1.90	1.78 ± 0.15	45.63	44.70	1.36	0.20
1453+3352 ^e	4.191	1.22	$2.39^{+0.56}_{-0.49}$	$1.38^{+0.35}_{-0.34}$	46.23	44.76	1.56	2.05
1511+5659	1.031	1.54	< 17.19	...	45.80	< 44.19	> 1.62	0.61
1515+5521	1.844	1.44	$4.02^{+1.63}_{-1.44}$	$4.56^{+0.90}_{-0.90}$	45.30	44.16	1.44	0.33
1539+4313	0.348	2.03	64.94 ± 2.34	1.96 ± 0.06	44.27	43.63	1.24	...
1543+5405	0.245	1.31	58.57 ± 5.41	2.08 ± 0.15	44.28	43.22	1.41	...
1545+4846	0.400	1.61	139.3 ± 10.9	2.23 ± 0.13	45.59	44.06	1.59	...
1605-0109	1.573	8.88	28.07 ± 3.18	2.03 ± 0.18	45.85	44.85	1.38	0.62
1618+3456	1.922	1.46	$7.21^{+1.96}_{-1.66}$	$1.76^{+0.44}_{-0.42}$	46.10	44.46	1.63	1.60
1640+4644	0.537	1.74	20.91 ± 0.73	2.13 ± 0.06	45.07	43.56	1.58	0.36
1641+4649	0.695	1.77	19.47 ± 1.22	2.11 ± 0.11	44.79	43.81	1.38	0.67
1641+4000	1.003	1.02	12.38 ± 0.95	1.74 ± 0.12	45.72	44.02	1.65	0.63
1657+3524	2.329	1.75	4.55 ± 0.68	1.69 ± 0.24	45.85	44.41	1.55	0.45
1701+6412	2.736	2.59	14.40 ± 0.93	2.04 ± 0.10	47.41	45.15	1.86	0.37
1702+3405	2.038	2.04	2.55 ± 0.29	1.37 ± 0.16	46.01	43.97	1.78	1.11
1703+6045	0.285	2.32	49.18 ± 3.43	2.18 ± 0.13	44.04	43.27	1.30	...
1708+6154	1.415	2.49	65.18 ± 4.69	2.00 ± 0.14	46.03	45.11	1.35	1.15
1719+2732	1.447	3.68	28.89 ± 3.64	2.22 ± 0.21	45.72	44.80	1.35	1.11
1720+2638	1.141	3.86	10.63 ± 0.94	2.40 ± 0.15	45.33	44.10	1.47	0.20
1735+5355	0.956	3.39	59.55 ± 3.96	1.98 ± 0.12	45.62	44.65	1.37	1.01

Table 4—Continued

Source	Redshift	Gal. N_H^a 10^{20} cm^{-2}	n_0^b $10^{-6} \text{ cm}^{-2} \text{ s}^{-1} \text{ keV}^{-1}$	Γ_X^c	$\log \nu L_\nu(2500 \text{ \AA})$ ergs s^{-1}	$\log \nu L_\nu(2 \text{ keV})$ ergs s^{-1}	α_{ox}	α_{UV}^d
1737+5828	1.776	3.51	$14.65^{+3.51}_{-3.03}$	$2.39^{+0.40}_{-0.38}$	45.80	44.68	1.43	0.79
1738+5837	1.279	3.59	$3.04^{+1.16}_{-0.94}$	$2.23^{+0.55}_{-0.53}$	45.97	43.66	1.89	1.41
2215-1611	3.990	2.65	$5.23^{+1.53}_{-1.29}$	$1.30^{+0.38}_{-0.38}$	46.81	45.05	1.68	0.80
2238-0921	3.259	4.64	< 23.19	...	46.70	< 45.50	> 1.46	0.31
2238-0937	1.472	4.78	< 69.50	...	45.58	< 45.17	> 1.16	1.07
2239-0933	1.818	4.63	< 57.74	...	45.84	< 45.30	> 1.21	0.63
2249-0808	0.457	3.46	55.44 ± 4.29	1.81 ± 0.11	44.11	43.86	1.09	...
2337+0025	2.054	3.81	$6.89^{+1.59}_{-1.39}$	$2.29^{+0.47}_{-0.43}$	45.87	44.50	1.53	0.18
2337+0022	1.376	3.30	$3.87^{+1.46}_{-1.18}$	$2.93^{+0.70}_{-0.65}$	45.48	43.85	1.63	0.99
2337+0026	1.703	3.80	21.37 ± 3.03	2.67 ± 0.28	45.84	44.90	1.36	0.15
2348+0107	0.718	3.98	28.51 ± 1.28	2.05 ± 0.08	45.19	44.01	1.45	0.32
2357+0043 ^e	4.362	3.33	$2.00^{+0.51}_{-0.44}$	$1.58^{+0.40}_{-0.38}$	46.54	44.72	1.70	1.74

Note. — Quoted errors are at 68% (1σ) confidence.

^aGalactic N_H , inferred from COLDEN (Dickey & Lockman 1990).

^bWhen fitting n_0 for the sources with < 50 counts, we fix $\Gamma_X = 1.9$.

^cThe photon index could not be estimated for those sources with upper limits.

^dThe UV spectral slope could not be estimated for sources with $z < 0.5$.

^eOne of seven new *Chandra* observations.

Table 5. Behavior of Kendall's Generalized Partial τ From Simulation

ρ^a	τ_{lz}^b	$\tau_{xz,l}^c$	$H_0 : L_X \propto L_{UV}^{0.65}$			$\tau_{xz,l}^c$	$H_1 : L_X \propto L_{UV}^{0.4} e^{-t(z)/5.5}$		
			$\text{pow}(\tau_{xz,l} H_0)^d$	$\tau_{\alpha z,l}^e$	$\text{pow}(\tau_{\alpha z,l} H_0)^f$		$\text{pow}(\tau_{xz,l} H_1)^d$	$\tau_{\alpha z,l}^e$	$\text{pow}(\tau_{\alpha z,l} H_1)^f$
0.9	0.715	0.153	0.988	0.105	0.845	0.290	1.000	0.011	0.061
0.6	0.412	0.101	0.696	0.074	0.390	0.338	1.000	-0.126	0.935
0.3	0.197	0.048	0.196	0.038	0.126	0.329	1.000	-0.204	1.000
0.0	0.000	0.000	0.050	0.000	0.050	0.299	1.000	-0.258	1.000

^aThe correlation between l_{UV} and $\log z$ used for the simulation.

^bThe average value of Kendall's τ between L_{UV} and z .

^cThe average value of Kendall's generalized partial τ between L_X and z , controlling for L_{UV} . The left value of $\tau_{xz,l}$ corresponds to when the null hypothesis, H_0 , is true, and the right value corresponds to when the alternative hypothesis, H_1 , is true.

^dThe power of the test when $\tau_{xz,l}$ is used and the null hypothesis H_0 is true (left) or the alternative hypothesis H_1 is true (right).

^eSame as $\tau_{xz,l}$, but when using α_{ox} instead of L_X .

^fSame as $\text{pow}(\tau_{xz,l}|\cdot)$, but when using $\tau_{\alpha z,l}$ instead of $\tau_{xz,l}$.